IMPROVING PLASMA ACTUATOR PERFORMANCE AT LOW PRESSURE, AND AN ANALYSIS OF THE POINTING CAPABILITIES OF CUBESATS USING PLASMONIC FORCE PROPULSION (PFP) THRUSTERS

by

PAUL DANIEL FRIZ

A THESIS

Presented to the Faculty of the Graduate School of the

MISSOURI UNIVERSITY OF SCIENCE AND TECHNOLOGY

In Partial Fulfillment of the Requirements for the Degree

MASTER OF SCIENCE IN AEROSPACE ENGINEERING

2014

Approved by

Joshua Rovey, Advisor
Henry Pernicka
Xiaodong Yang

PUBLICATION THESIS OPTION

This thesis has been prepared in the form of one paper and one report. The paper entitled *The Effects of Electrode Size and Configuration on Plasma Actuator Thrust and Effectiveness at Low Pressure* was accepted for publication in the International Journal of Flow Control and therefore have been prepared in the aforementioned journal style. The second section is a report on the development and use of Plasmonic Force Propulsion (PFP) thrusters prepared in the standard thesis style.

ABSTRACT

This thesis details the work done on two unrelated projects, plasma actuators, an aerodynamic flow control device, and Plasmonic Force Propulsion (PFP) thrusters, a space propulsion system for small satellites.

The first half of the thesis is a paper published in the International Journal of Flow Control on plasma actuators. In this paper the thrust and power consumption of plasma actuators with varying geometries was studied at varying pressure. It was found that actuators with longer buried electrodes produce the most thrust over all and that they substantially improved thrust at low pressure. In particular actuators with 75 mm buried electrodes produced 26% more thrust overall and 34% more thrust at low pressure than the standard 15 mm design.

The second half details work done modeling small satellite attitude and reaction control systems in order to compare the use of Plasmonic Force Propulsion thrusters with other state of the art reaction control systems. The model uses *bang bang* control algorithms and assumes the worst case scenario solar radiation pressure is the only disturbing force. It was found that the estimated 50-500 nN of thrust produced by PFP thrusters would allow the spacecraft which use them extremely high pointing and positioning accuracies ($<10^{-9}$ degrees and 3×10^{-12} m). PFP thrusters still face many developmental challenges such as increasing specific impulse which require more research, however, they have great potential to be an enabling technology for future NASA missions such as the Laser Interferometer Space Antenna, and The Stellar Imager.

ACKNOWLEDGMENTS

First, I would like to thank Dr. Joshua Rovey for being my advisor, and for your guidance and motivation. Thank you for allowing me to do an unorthodox thesis covering two unrelated topics. Without this I would still be studying plasma actuators, but instead was given the opportunity to develop innovative new space technology. Thank you Dr. Henry Pernicka and Dr. Xiaodong Yang for being on my thesis committee. I also want to thank past teachers who have allowed me to get this far. Particularly Dr. Vayujeet Gokhale for supporting my undergraduate research in astronomy, Dr. Peter Rolnick for encouraging me to continue studying physics when I was struggling, and Dr. Andrew Shaw for encouraging me to pursue a degree in the sciences.

Professionally I would like to thank Lockheed Martin Missile and Fire Control for funding my initial research in plasma actuators, and the NASA Innovative Advanced Concepts (NIAC) program, and NASA-Missouri Space Grant Consortium for funding my research on PFP thrusters. Also, I would like to thank Crown Audio for donating an amplifier after I blew up all the others in the AP lab. My work on PFP thrusters would not have been possible without the guidance from Dr. Rovey and Dr. Yang, and the work done by Matthew Glascock and Changyu Hu.

Personally I would like to thank all my friends and family for their support and encouragement, you guys are the best.

Now, as is tradition in the AP lab, I will begin the "tongue-in-cheek" acknowledgments. I would like to thank my fellow "top grad students" in AP lab for the lively discussions and help along the way, particularly Warner who's constant discouragement and general gripery has actually been quite uplifting, and Ryan, who spared me my usual fate of being "that guy in the lab who everyone picks on." Finally, I would like to impart some advice given to me by Dr. Rovey on a particularly frustrating day in the lab after I accidentally melted a plasma actuator. After I described the problem he considered it for a moment and said "You need to find a way to make it stop doing that..." Upon further consideration he added "Try adding more Kapton." From this I learned that pretty much any experimental problem can be solved by adding more Kapton tape and that the proper explanation for any problem is "It's because of the Plasma!"

TABLE OF CONTENTS

Page

LIST OF ILLUSTRATIONS

LIST OF TABLES

1. INTRODUCTION

This thesis details the work completed on two separate and unrelated projects. The first work completed was a study conducted to improve the thrust generated by plasma actuators at low pressure. This work has been accepted for publication in the International Journal of Flow Control the aforementioned publication is presented as the first half of this thesis. The second project involved utilizing *bang bang* control algorithms in order to determine the best theoretical pointing and positioning precision of cubeSats employing Plasmonic Force Propulsion (PFP) thrusters. This work was the third part in a three part study funded by the NASA Innovative Advanced Concepts (NIAC) program. The goal of this study was to show whether or not PFP thrusters are a viable attitude or reaction control system for cubeSats and other small spacecraft.

Plasma actuators are an experimental flow control device which use plasma to alter the flow fields around them. They have a number of possible applications currently being studied including: reduction of flow separation on airfoils at high angle of attack[1], separation control on turbine blades[2], controlling Micro and Unmanned Aerial Vehicles (μAVs) and (UAVs)[3] and control of the phantom yaw experienced by missile bodies at high angle of attack due to asymmetric vortex shedding. The main advantage of plasma actuators over traditional flow control devices is that they have no moving parts and can be turned on and off almost instantaneously[4].

Their design, seen in Figure 1.1, is very simple and consists of two asymmetrically placed electrodes separated by an insulating or dielectric material. The exposed electrode, marked *a* in Figure 1.1 is driven by a high voltage AC waveform typically at 1-15 kHz and 12-20 kVpp[5–10]. The buried electrode, marked *b* in Figure 1.1 is grounded. The resulting strong and oscillating electric field between the exposed and buried electrode causes electrons to fly off the exposed electrode. These electrons then collide with the

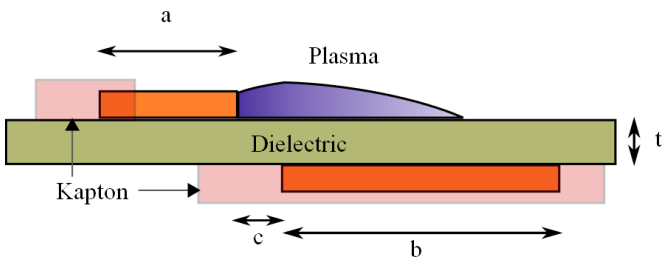

Figure 1.1: Common plasma actuator design.

surrounding air particles turning them into plasma. That plasma is then accelerated away from the exposed electrode by the electric field creating a small thrust on the order of a few millinewtons. While the thrust is very small it can be enough to alter the flow field around an airfoil significantly.[1]

As pressure decreases the thrust produced by plasma actuators initially increases but as pressure is decreased below 80 kPa the thrust production decreases significantly.[6] The goal of this study was to increase the thrust produced by plasma actuators at low pressure. The study investigated the effects of varying the geometry of the electrodes on thrust at low pressure: specifically by altering the lengths of the exposed and buried electrodes, marked *a* and *b* respectively, in Figure 1.1, and the chord wise gap between them, marked *c*. It was found that increasing the length of the buried electrode *b* had the largest effect on thrust overall and at low pressure. In particular actuators with 75 mm buried electrodes produced 26% more thrust overall and 34% more thrust at low pressure than the standard 15 mm design.

Plasmonic Force Propulsion thrusters are a previously unexplored propulsion device which use the plasmonic interaction between light and sub-wavelength sized metallic nanostructures to accelerate nanoparticles creating thrust. Plasmonics is the study of the oscillation of surface electrons caused by the interaction between light and the surfaces of metals. Previously "optical tweezers" which use optical forces similar to those used by

PFP thrusters have been used by biologists to pickup and move viruses.[11, 12] Plasmonic forces can be used to either trap nanoparticles, in a similar fashion to "optical tweezers" or accelerate them depending on the shape of the potential function related to the plasmonic force.[13, 14]

PFP thrusters will operate by constructing asymmetric sub-wavelength gold nanostructures, seen in Figure 1.2 which resonate with particular wavelengths of light. The light resonates more strongly with the wider end of the structure than the narrower end. This asymmetric resonance creates an electric field gradient which will then be used to accelerate nanoparticles at high speeds. By combining arrays of millions of these structures into a thruster seen in Figure 1.3 it is possible to create thrusts on the order of 50-500 nN with specific impulses varying from 1-12 s. Each layer of nanostructures will be designed to resonate with a different wavelength of light thus taking advantage of the entire solar spectrum. Thruster designs will be easily customizable by changing the dimensions of the array, but will be on the order of millimeters long and tens to hundreds of microns thick. To put this in perspective each thruster will be about the size of a human hair.

The small size of PFP thrusters makes them ideal for small spacecraft such as cubeSats. The low thrust of PFP thrusters makes them ideal for applications such as ultra fine pointing for space telescopes and ultra fine positioning for formation flying satellites. The proposed NASA mission known as the Laser Interferometer Space Antenna

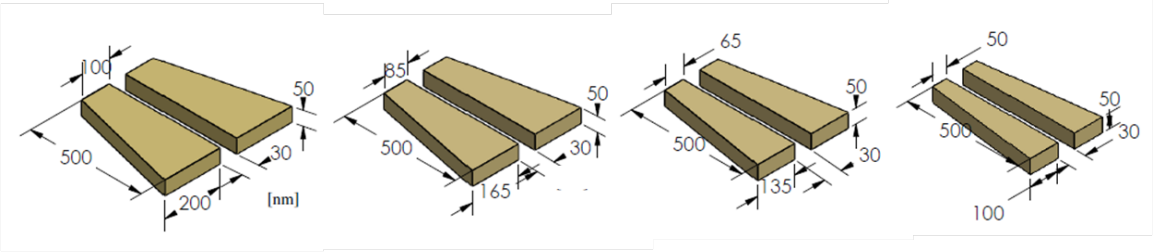

Figure 1.2: Sub-wavelength gold nanostructures designed to resonate with different wavelengths of incident light.

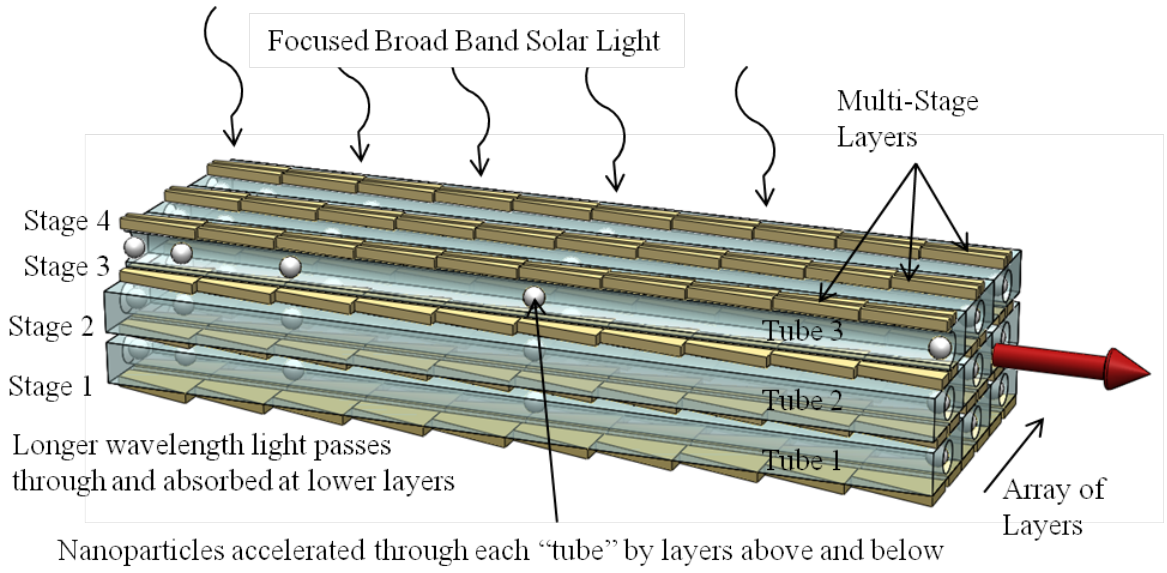

Figure 1.3: Diagram of the proposed PFP thruster design.

or LISA requires that three spacecraft each be able to adjust their relative positions to within picometers.[15–17] This will only be possible with and extremely low thrust reaction control system such as PFP thrusters. PFP thrusters could also be used on future NASA space telescopes such as the Stellar Imager or SI. The SI mission concept is to use an array of 20-30 small "mirror sats" each with a 1 m mirror segment positioned over several kilometers to form an extremely high resolution ultraviolet interferometric telescope. The resolution of the SI will be 0.1 milliarcseconds which is so high it will be able to image the surfaces of other stars. In order to achieve such high resolution each "mirror sat" will need to be positioned to an accuracy of nanometers and control its attitude to within 0.76 milliarcseconds.[18–20] Such high attitude and position control capabilities are not currently possible but could be with enabling technologies such as PFP thrusters.

The work presented in this thesis on PFP thrusters is the third part in a three part study funded by the NIAC program. The first part of the study is to quantify the forces produced on nanoparticles by structures shown in Figure 1.2 at varying intensities of solar light. The second part is to determine the thrust and specific impulse of various arrays

of nanostructures as seen in Figure 1.3. The third part is to determine the pointing and positioning capabilities of cubeSats employing PFP thrusters and compare them to other state of the art micropropulsion systems. This thesis provides a summary of the results of parts one and two but primarily focus on the attitude and proximity control modeling done by the author.

PAPER

1. THE EFFECTS OF ELECTRODE SIZE AND CONFIGURATION ON PLASMA ACTUATOR THRUST AND EFFECTIVENESS AT LOW PRESSURE

Paul D. Friz and Joshua L. Rovey

Missouri University of Science and Technology, Rolla, Missouri, 65401, USA

ABSTRACT

The thrust production and power consumption of plasma actuators with varying electrode geometries was measured. The geometries were varied by changing the chord-wise length of the exposed and buried electrodes as well as varying the chord-wise gap between the electrodes. Each actuator was driven with a 5 kHz sine wave at 16 kVpp, and operated at pressures ranging from 10-101 kPa, which corresponds to altitudes from 16,000 m to sea level. The electric field of each configuration was also modeled using Maxwell Ansoft. Increasing the length of the buried electrode was found to have the greatest effect on thrust production especially at low pressure. Actuators with 75 mm buried electrodes produced an average of 26% more thrust at all pressures and 34% more thrust at 20-40 kPa than the traditional 15 mm buried electrode. The gap study revealed that actuators with a 1 mm gap produced the most thrust at all pressures. All actuator designs were found to have a similar linear relationship between their effectivenesses and operating pressure.

NOMENCLATURE

a Chord-wise exposed electrode length, mm

b Chord-wise buried electrode length, mm

c Chord-wise gap between exposed and buried electrodes, mm

t Thickness of dielectric material, mm

p Pressure, kPa

F Thrust, mN

P Power, W

V Voltage, kVpp

I Current, mA

ξ Effectiveness, mN/W

1.1. INTRODUCTION

Single Dielectric Barrier Discharge (SDBD) plasma actuators are a promising flow control device for a variety of aerospace applications. Applications of plasma actuators include: reduction of flow separation on airfoils at high angle of attack[1], separation control on turbine blades[2], controlling Micro and Unmanned Aerial Vehicles (μAVs) and (UAVs)[3] and control of the phantom yaw experienced by missile bodies at high angle of attack due to asymmetric vortex shedding. The main advantage of plasma actuators over traditional flow control devices is that they have no moving parts and can be turned on and off almost instantaneously[4].

A SDBD plasma actuator consists of two electrodes separated by a dielectric in an asymmetric configuration shown in Figure 1.4. The electrodes are usually copper or aluminum tape placed directly on the dielectric. Common dielectrics include but are not limited to Teflon, Kapton, fiberglass epoxy, and Macor[5–8]. The buried electrode is electrically grounded and encapsulated in a second dielectric. In this and many other studies Kapton tape is used as the dielectric material to encapsulate the buried electrode thus preventing electrical discharge and plasma formation on the back side of the actuator. The exposed electrode is typically driven by an AC waveform of 1-15 kHz and 12-20 kVpp[5–

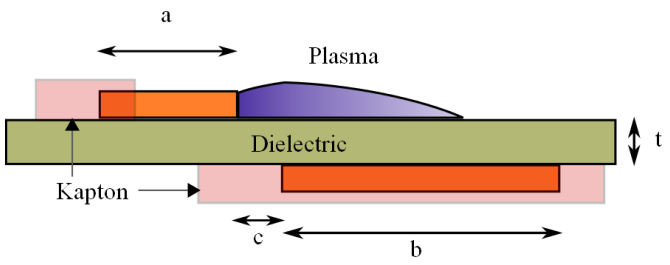

Figure 1.4: Plasma actuator design used in this study.
The lengths a, b, and c were independently varied.

10]. The AC cycle of the actuator is commonly divided into two sections; the forward stroke, when the voltage on the exposed electrode is negative going, and the backward stroke, when the voltage is positive going. During the forward stroke the electrons emitted from the exposed electrode collide with neutral air particles ionizing them. Those ions are then accelerated away from the exposed electrode and collide with the surrounding air thus inducing what is called ionic wind. During the backward stroke electrons return to the exposed electrode coming off the dielectric surface, again colliding with air particles creating plasma[7, 8, 21]. It has been shown that 97% of the momentum coupling between the plasma and air occurs during the forward stroke and that negative oxygen ions are primarily responsible for the momentum transfer[22]. Because time resolved measurements of the actuator thrust production are difficult to obtain it is still not clear if the plasma actuator pushes ions away in both the forward and backward stroke or if it pushes ions during the forward stroke but weakly pulls ions back during the backward stroke[22].

If plasma actuators are to be used on aircraft and missiles they must first be demonstrated to be capable of producing enough thrust to provide control at the low pressures found at high altitudes. Abe *et al.* demonstrated that for a plasma actuator with exposed and buried electrode lengths of 15 mm separated by fiberglass epoxy and a 1 mm chord-wise gap as pressure decreases the thrust production of the plasma actuator increases slightly. However, as pressure is decreased beyond 75 kPa, thrust production decreases

significantly[6]. Nichols measured the electric field of an actuator with a 50 mm buried electrode and showed that at low pressure up to 88% of the plasma is formed in regions where the electric field is relatively weak[7, 8]. A more recent study by Soni and Roy showed that the thrust vs pressure profile as well as the effectiveness (defined as unit of thrust produced per unit of power used) can be modified by changing the dielectric material, dielectric thickness, and applied voltage. Specifically they found that thrust is increased with decreasing dielectric thickness and that decreasing dielectric thickness pushes the peak of the thrust vs pressure profile to lower pressures[5]. The goal of this paper is to better explain why thrust decreases at low pressure and to develop methods of increasing thrust at low pressure.

The rest of this paper is divided into three main sections: Experimental Setup, Results, and Discussion. The Results and Discussion sections are each divided into three subsections examining the effects of varying buried electrode length, exposed electrode length, and the chord-wise gap length.

1.2. EXPERIMENTAL SETUP

The plasma actuator design used in the experiment is shown in Figure 1.4. The insulating dielectric has a thickness t=1.54 mm, and is made of G-10 glass epoxy with dielectric constant $\varepsilon_r = 4.9$. The electrodes are made of 0.04 mm thick copper tape spanning 240 mm and are placed on either side of the dielectric and separated by a gap of $c = 1$ mm. The chord length of the exposed and buried electrodes vary and are denoted a and b, respectively. The exposed electrode is driven with a 5 kHz 16 kVpp sinusoidal electrical signal, and its upstream edge is covered in Kapton tape to prevent any reverse discharges. The buried electrode is electrically grounded and is completely covered in multi-layered Kapton tape to prevent any electrical discharge on the back of the actuator.

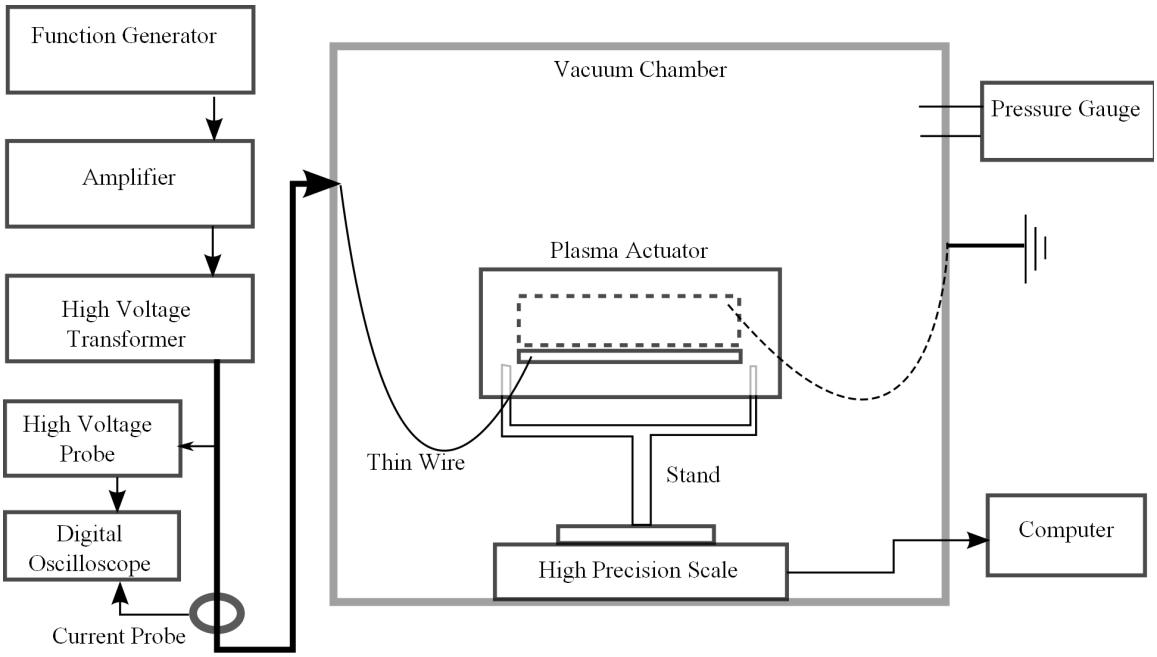

Figure 1.5: Schematic of the experimental setup.

A schematic of the experimental setup is provided in Figure 1.5. A Rigol DG1022 function generator provides the 5 kHz sinusoidal signal. The signal is then amplified by a Crown CE 2000 amplifier and sent to a Corona Magnetics CMI-5525-2 transformer. The voltage and current output from the transformer is monitored by a North Star PVM-5 high voltage probe and a Pearson Electronics model 4100 current monitor. A high voltage line carries the now 5 kHz 16 kVpp signal from the output of the transformer into the vacuum chamber. A lightly insulated 0.25 mm diameter wire connects the high voltage wire to the exposed electrode of the plasma actuator so that the heavy high voltage wire does not interfere with thrust measurements. A similar wire grounds the buried electrode to the vacuum chamber which is in turn grounded to the building. The vacuum chamber has an inner diameter and length of 0.60 m and 0.70 m respectively. The pressure within the chamber is monitored by a Kurt J. Lesker KJL275800 thermocouple gauge. The KJL275800 is accurate to $\pm 2.5\%$ above 50 kPa, below 50 kPa it is only accurate to $\pm 10\%$. For the sake of clarity pressure error bars are omitted on all graphs in this report.

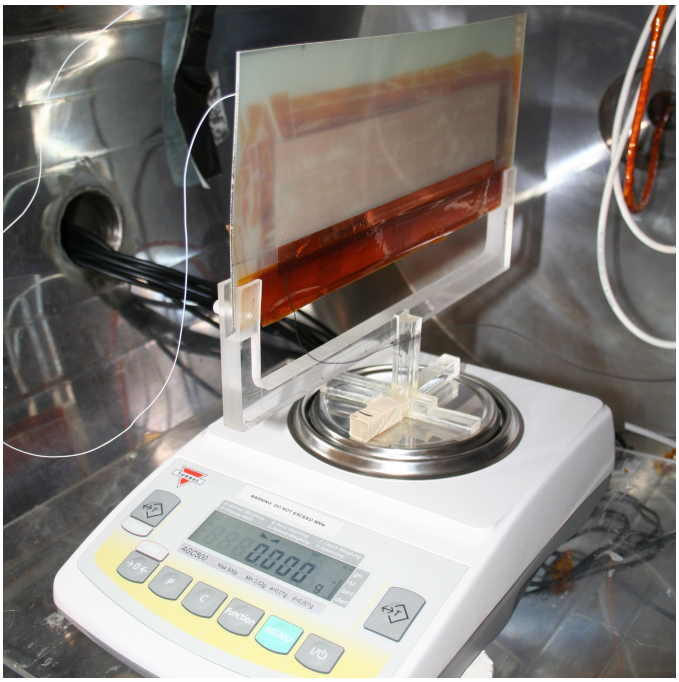

Figure 1.6: Photo of a plasma actuator mounted on the acrylic stand on top of the scale.

The plasma actuator is placed on an acrylic stand on a Torbal AGC500 scale as seen in Figure 1.6. Traditionally plasma actuators are mounted in such a way that that the plasma discharge points down. However, it was found that when the actuators were mounted in this fashion the acrylic stand blocked some of the ionic wind causing inaccurate measurements. To solve this the actuators were mounted upside down so that they were discharging up. Thrust measurements were obtained by averaging two sets of ten measurements taken over ten seconds from the scale and the errors reported are the standard deviation of those measurements. The current and voltage readings were acquired using a Tektronix DPO 2024 oscilloscope. The current and voltage waveforms were multiplied and averaged by the oscilloscope to obtain the average power measurements. The power measurements were found to vary by $\pm 10\%$ for any given pressure and driving voltage.

1.3. RESULTS

To gain confidence in the accuracy of the thrust measurements, a plasma actuator with the same dielectric material and electrode configuration as the design of Abe *et al.* was constructed. The only differences between the two were that the new actuator dielectric had a thickness of 1.54 mm as opposed to Abe's, which was 1.80 mm thick and the electrodes spanned only 240 mm whereas Abe's spanned 300 mm. The actuator was driven at 5 kHz 20 kVpp and its Thrust/Length was found to be consistent with the measurements of Abe *et. al.* and Soni and Roy (Figure 1.7). Soni and Roy reported that decreasing the thickness of the actuator dielectric increases its thrust production which accounts for why the thrust measurements of Soni and Roy, and those obtained in this experiment were on average 18% and 12% higher than that of Abe, respectively[5, 6].

The results of this geometry study are divided into three sections, each showing how varying one geometric parameter affects actuator thrust production and effectiveness.

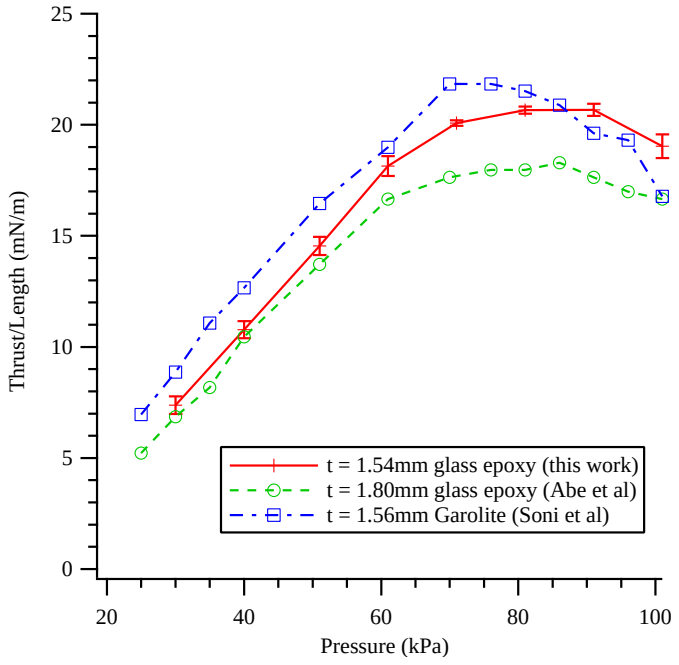

Figure 1.7: Comparison of thrust measurements with that of Abe and Soni.

In the following section, the actuator buried electrode length, exposed electrode length and chord-wise gap length are varied.

1.3.1. Buried Electrode Study. In this study, the electric field and capacitive effects of the plasma actuator were altered by changing the chord-wise length of the buried electrode. Five separate plasma actuators were constructed with 15 mm exposed electrodes and buried electrodes measuring $b = 8$ mm, 15 mm, 30 mm, 50 mm, and 75 mm. Each actuator had a 1 mm chord-wise gap between the exposed and buried electrodes. The exposed electrode was driven at 5 kHz, 16 kVpp. The thrust and effectiveness profiles are shown in Figures 1.8 and 1.9 . Initially, as buried electrode length increases the thrust production at low pressures increases but decreases at higher pressures. However, as the buried electrode length is extended to 50 mm and beyond production is increased at all pressures. The 75 mm buried electrode actuator produced an average of 26% more thrust at all pressures and 34% more thrust at 20-40 kPa than the traditional 15 mm buried electrode actuator. No

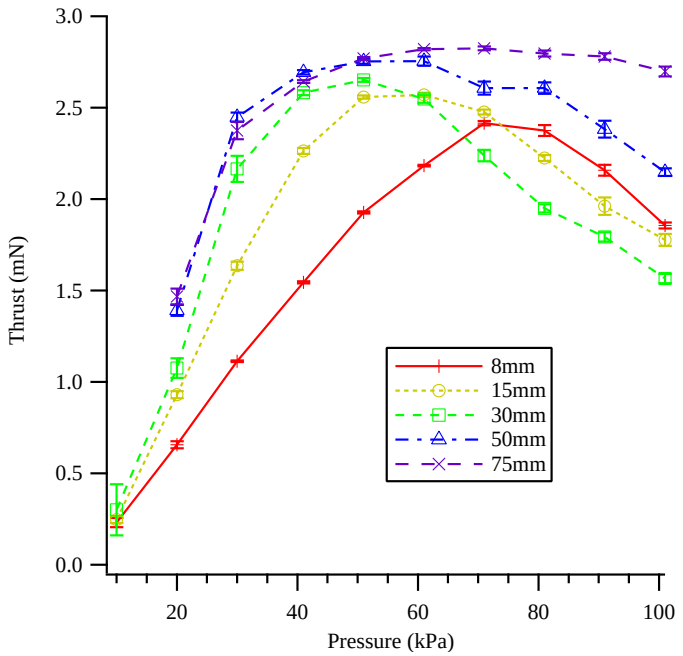

Figure 1.8: Thrust profiles of actuators with different buried electrode lengths but fixed exposed electrode length and gap length of 15 mm and 1 mm respectively.

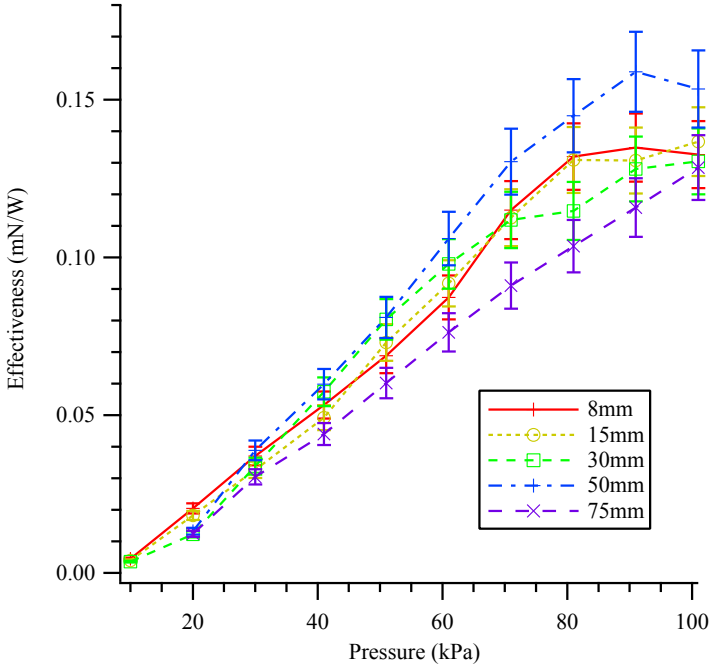

Figure 1.9: Effectiveness profiles of actuators with different buried electrode lengths but fixed exposed electrode length and gap length of 15 mm and 1 mm respectively.

clear relationship between buried electrode length and the effectiveness profile is apparent; however, the $b = 50$ mm actuator was the most effective at all pressures and the $b = 75$ mm actuator was the least effective. No thrust or effectiveness data was taken at 15 kPa for the $b = 50$ and 75 mm actuators because the amplifier was not capable of supplying the necessary current without severely overheating.

1.3.2. Exposed Electrode Study. In this study the thrust and effectiveness profiles were obtained for actuators with exposed electrodes of length $a = 10$ mm, 15 mm, and 20 mm. The results of this study are shown in Figures 1.10 - 1.13. To ensure consistency the test was conducted on actuators with buried electrodes of length $b = 15$ mm and 75 mm. Again the actuators were driven at 5 kHz, 16 kVpp. The results in Figures 1.10-1.13 show that altering the exposed electrode length has little effect on both thrust and effectiveness. At high pressures the $a = 15$ mm and $a = 10$ mm electrode thrust and effectiveness profiles are nearly identical as seen in Figures 1.10 and 1.11 corresponding to $b = 15$ mm. While

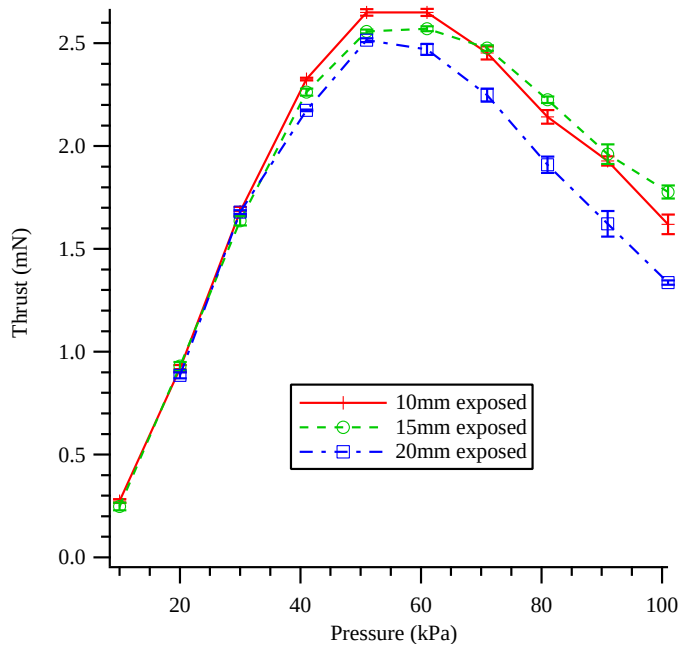

Figure 1.10: Thrust profiles of actuators with different exposed electrode lengths, fixed gap of 1 mm, and buried electrode length of 15 mm.

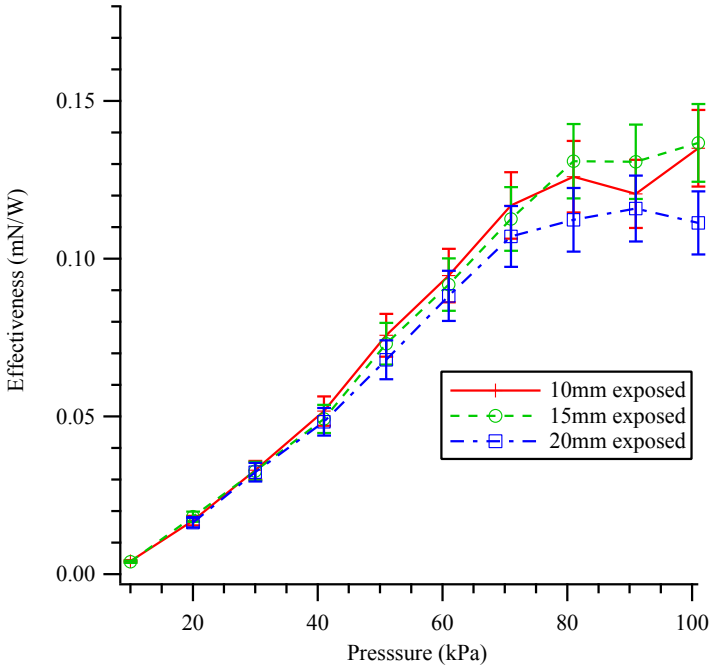

Figure 1.11: Effectiveness profiles of actuators with different exposed electrode lengths, fixed gap of 1 mm, and buried electrode length of 15 mm.

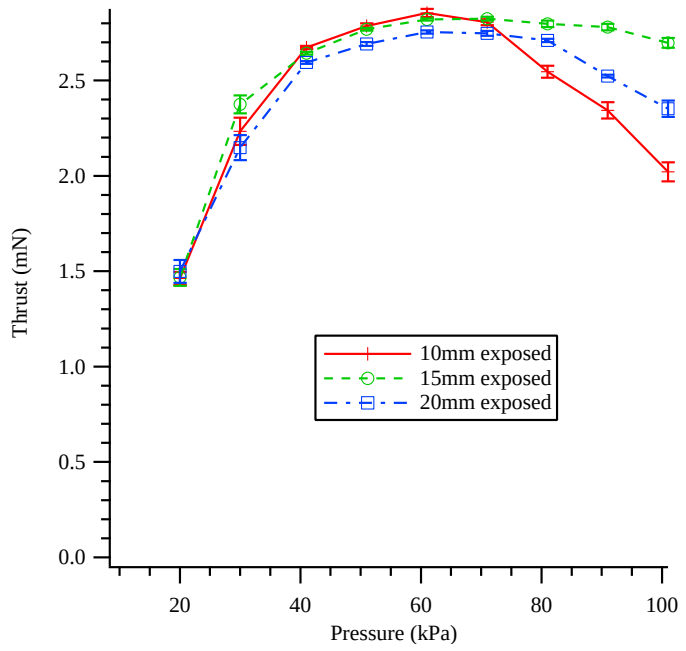

Figure 1.12: Thrust profiles of actuators with different exposed electrode lengths, fixed gap of 1 mm, and buried electrode length of 75 mm.

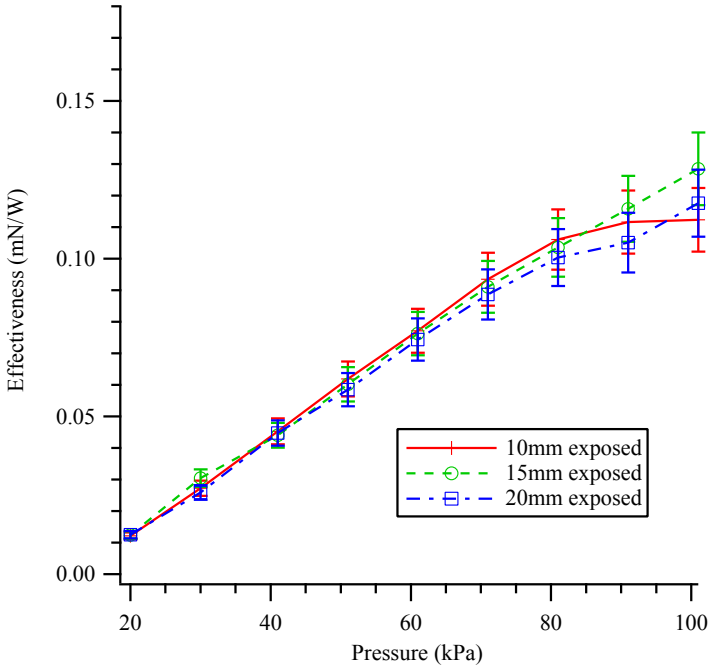

Figure 1.13: Effectiveness profiles of actuators with different exposed electrode lengths, fixed gap of 1 mm, and buried electrode length of 75 mm.

increasing the exposed electrode length from $a = 15$ mm to $a = 20$ mm decreases average thrust production above 60 kPa by 13% and average effectiveness by 11%. Figures 1.12 and 1.13 show that the exposed electrode length does not affect thrust production for actuators with $b = 75$ mm for pressure at and below 70 kPa. However, above 70 kPa the $a = 15$ mm produced on average 8% and 16% more thrust than the $a = 20$ mm and $a = 10$mm actuators respectively. Exposed electrode length had no noticeable effect on effectiveness for $b = 75$ mm actuators.

1.3.3. Gap Study. In this study two actuators with exposed electrodes $a = 15$ mm and buried electrodes $b = 15$ mm and $b = 75$ mm were studied. Thrust and effectiveness profiles were obtained for chord-wise gaps of $c = -3$ mm, 1 mm, and 3 mm. The results of this study are shown in Figures 1.14 - 1.17. All other parameters remained the same as in the buried and exposed electrode studies. Figures 1.14 and 1.16 shows that changing the gap length from $c = 1$ mm to $c = -3$ or 3mm decreases thrust production for both the

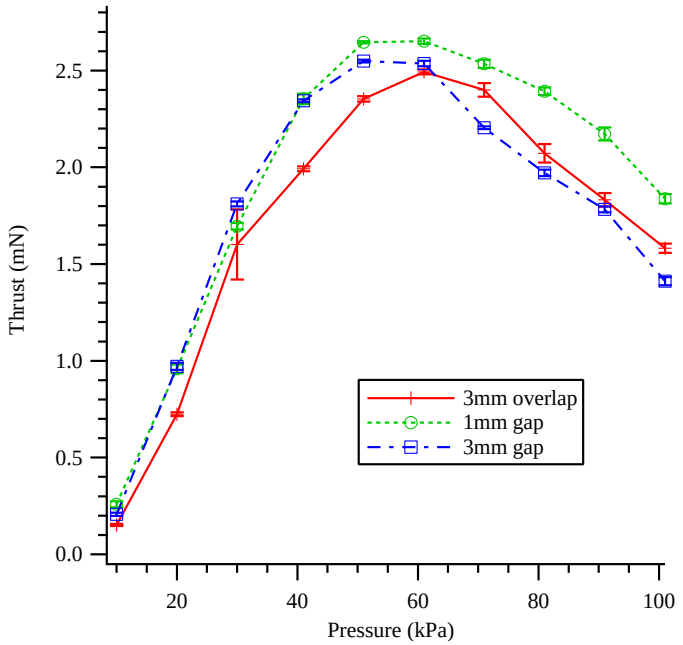

Figure 1.14: Thrust profiles of actuators with 15 mm exposed and buried electrodes and varying gap lengths.

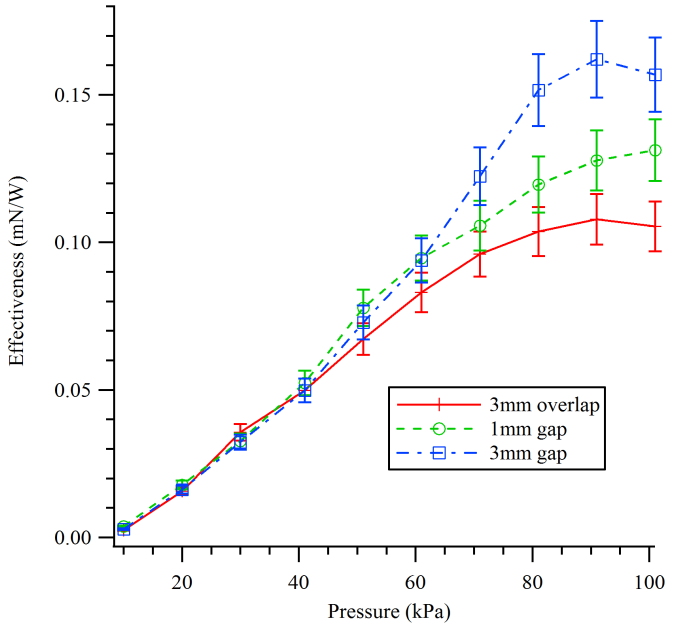

Figure 1.15: Effectiveness profiles of actuators with 15 mm exposed and buried electrodes and varying gap lengths.

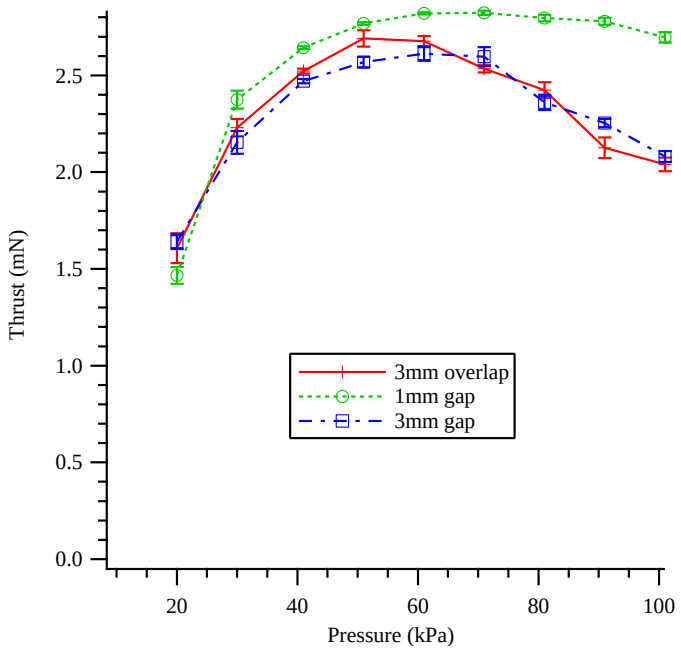

Figure 1.16: Thrust profiles of actuators with 15 mm exposed and 75 mm buried electrodes and varying gap lengths.

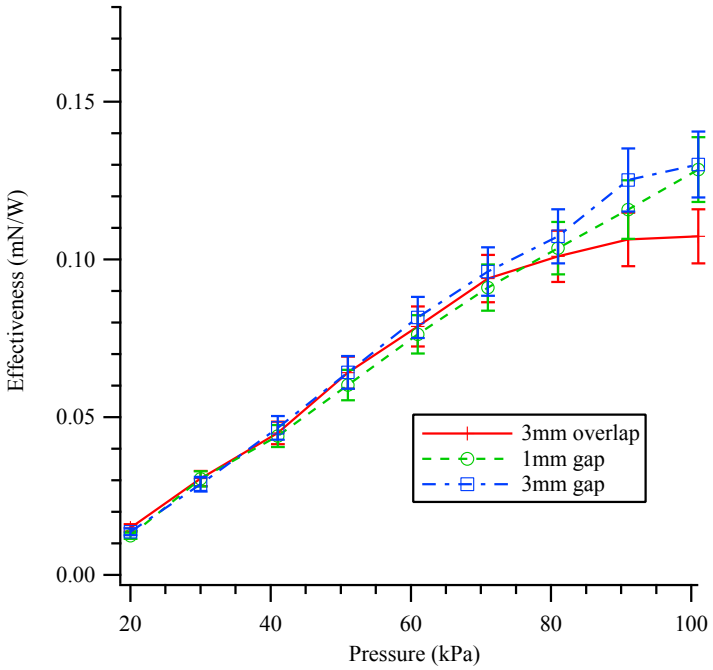

Figure 1.17: Effectiveness profiles of actuators with 15 mm exposed and 75 mm buried electrodes and varying gap lengths.

$b = 75$ mm and 15 mm actuators. For buried electrode length $b = 75$ mm, the $c = -3$ mm and 3mm designs produced 10% less thrust than the $c = 1$ mm actuator, on average. For the $b = 15$ mm actuator the $c = -3$ mm design produced 12% less thrust and the $c = 3$ mm design produced 9% less thrust on average than the $c = 1$ mm design. Figure 1.15 shows that altering chord-wise gap had the greatest effect on the effectiveness of the actuators of all the previous geometric variations. The $b = 15$ mm $c = 3$ mm design was 13% more effective overall and was 22% more effective at 70 kPa and above. However, the $b = 75$ mm $c = 3$ mm design seen in Figure 1.17 did not improve effectiveness by any significant amount at any pressure.

1.4. DISCUSSION

The overall trends and the effects of altering electrode geometry on the electric field, thrust production and effectiveness are discussed in this section. The electric field of each actuator was computed using the finite element analysis software Maxwell Ansoft. The electric field solution plotted is only the electric field due to the voltage of the exposed electrode and the effects of the dielectric materials and buried electrode. They do not show the effects on the electric field due to charge buildup on the dielectric surface during discharge or the effects of the plasma. Previous studies have shown that both the electric field and the charge distribution on the dielectric play key rolls in producing plasma and thrust[7, 8, 21].

1.4.1. Effects of Varying Buried Electrode Length. It was expected that actuators with longer buried electrodes would produce more thrust at lower pressures because the electric field can maintain a greater magnitude farther downstream as seen in Figure 1.18. Figure 1.18 also shows that each actuator has the same magnitude of electric field up until the point where it reaches the end of its buried electrode at which point the electric field rises slightly due to edge effects then quickly falls off. Figure 1.19 shows the extent of the plasma formation as pressure decreases for actuators being driven at 16 kVpp with buried electrode lengths of $b = 8$ mm, 15 mm and 50 mm. Abe *et al.* and Soni and Roy separately demonstrated that as pressure is decreased the extent of the plasma over the buried electrode increases and that the extent of the plasma is limited to the length of the buried electrode[5, 6].

Figure 1.19 further illustrates those findings and shows that until the pressure reaches 50 kPa the primary factor limiting thrust production at low pressure is the extent of the electric field. Figure 1.8 shows that when the $b = 8$ mm actuator is driven at 16 kVpp it produces its maximum thrust at 70 kPa. As pressure decreases below 70 kPa the thrust production falls off quickly. In Figure 1.19b, which corresponds to $b = 8$ mm, and $p = 70$ kPa,

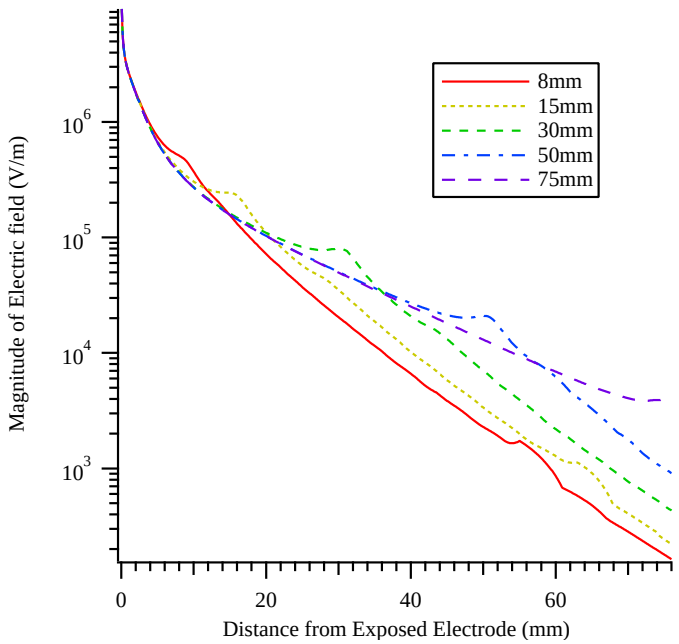

Figure 1.18: The modeled electric field of actuators with varying b just above the surface of the dielectric as a function of distance downstream from the exposed electrode.

the plasma has extended approximately 6 mm downstream from the exposed electrode. Figure 1.18 shows that edge effects of the buried electrode first occur 6 mm downstream of the exposed electrode. Similarly as seen in Figure 1.8 the $b = 15$ mm actuator reaches its maximum thrust production at $p = 50 - 60$ kPa. At 50 kPa the plasma has extended approximately 11 mm as seen in Figure 1.19g which also corresponds to the point on Figure 1.18 where the electric field starts to be effected by the edge of the buried electrode. Figure 1.8 also shows that the $b = 50$ mm actuator has its thrust maximum at 50 kPa, its plasma extends much farther at lower pressures as seen in Figure 1.19l. Below 50 kPa the thrust production decreases but not nearly as fast as with actuators with shorter buried electrodes. The previous study by Nichols measuring the combined electric fields of both the electrodes and the charge distribution on the surface of the dielectric using V-dot probes predicted that an actuator with a 50 mm buried electrode would produce the most thrust at 57 kPa and follow the general trends seen in Figure 1.8[7, 8].

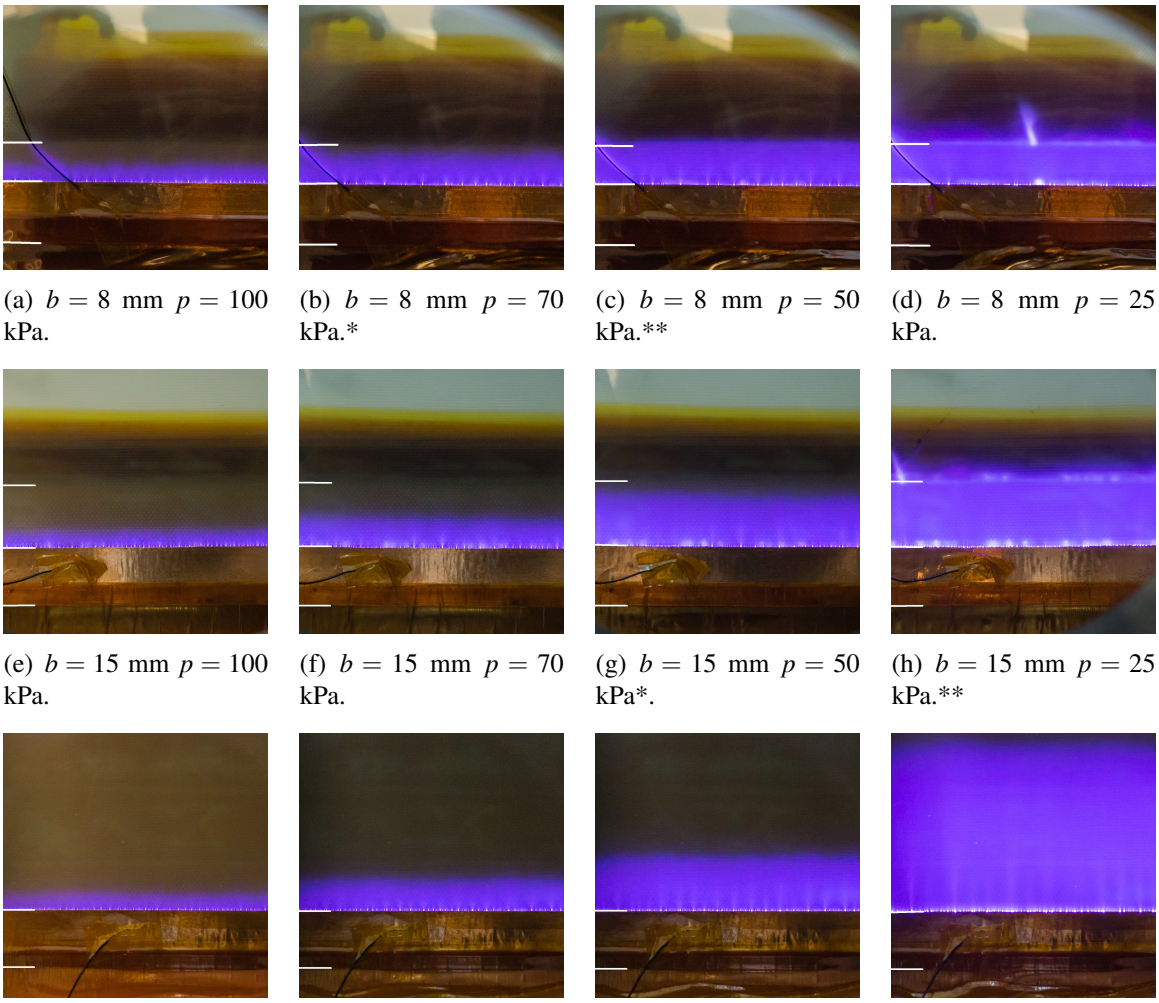

(a) $b = 8$ mm $p = 100$ kPa. (b) $b = 8$ mm $p = 70$ kPa.* (c) $b = 8$ mm $p = 50$ kPa.** (d) $b = 8$ mm $p = 25$ kPa.

(e) $b = 15$ mm $p = 100$ kPa. (f) $b = 15$ mm $p = 70$ kPa. (g) $b = 15$ mm $p = 50$ kPa*. (h) $b = 15$ mm $p = 25$ kPa.**

(i) $b = 50$ mm $p = 100$ kPa. (j) $b = 50$ mm $p = 70$ kPa. (k) $b = 50$ mm $p = 50$ kPa.* (l) $b = 50$ mm $p = 25$ kPa.

Figure 1.19: Plasma extent at 16 kVpp and varying pressure for plasma actuators with exposed electrode length 15 mm and buried electrode lengths of 8 mm, 15 mm and 50mm. The plasma brightens at the edge of the buried electrode outlining it as seen in (d) and (h). The edges of the buried and exposed electrodes are highlighted by the white lines.
*Pressure at which thrust production reaches maximum.
**Pressure at which plasma extent becomes limited by buried electrode length

Soni and Roy reported that, as pressure decreases, the effectiveness of actuators initially increases reaching a maximum at sub-atmospheric pressures then rapidly falls off as the pressure decreases further. However, the effectiveness profiles shown in Figure 1.9 linearly decrease as pressure is decreased in accordance with the previous study by Gregory

et.al[23]. However, Soni and Roy operated their actuators at 6-15 kVpp and their results indicated that actuator maximum effectiveness occurs at higher pressures as driving voltage is increased[5]. The $b = 8$ and $b = 50$ mm actuators in Figure 1.9 reach a maximum effectiveness at 90 kPa. This implies that if the pressure were increased above atmospheric pressure that the effectiveness would cease to follow the increasing linear trend and decrease.

1.4.2. Effects of Varying Exposed Electrode Length. The Maxwell Ansoft analysis showed no significant difference in electric field when altering the exposed electrode length as seen in Figure 1.20. This explains why changing the exposed electrode length has no large effect on thrust or effectiveness profiles.

1.4.3. Effects of Changing Chord-wise Gap Length. Figure 1.21 shows the change in the electric field near the exposed electrode as chord-wise gap is changed. The actuator with the electrodes overlapping has a stronger electric field closer to the exposed electrode

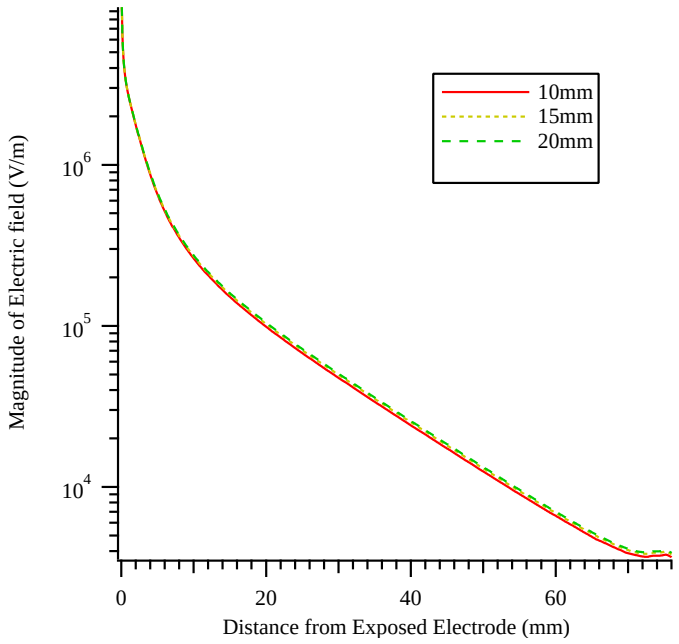

Figure 1.20: The simulated electric fields of actuators with varied exposed electrode length just above the surface of the dielectric as a function of distance downstream from the exposed electrode.

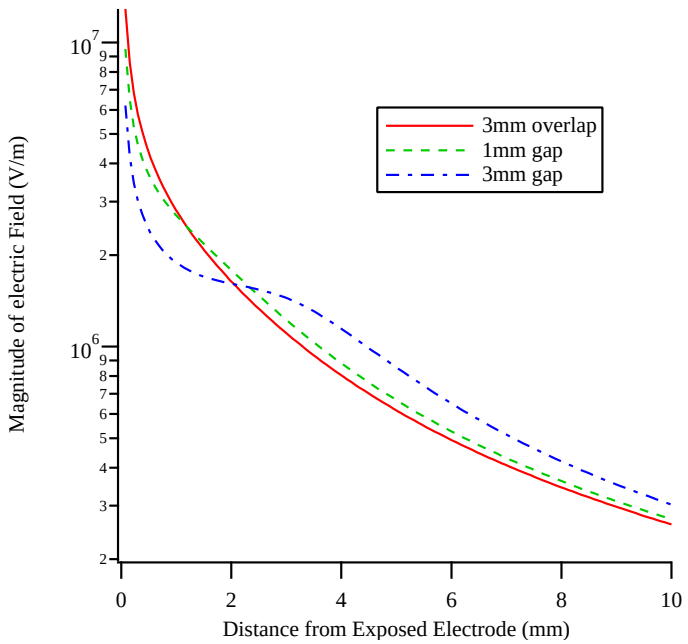

Figure 1.21: The simulated electric fields of actuators with varied gap length just above the surface of the dielectric as a function of distance downstream from the exposed electrode.

but drops off fastest moving downstream. The actuator with the 3 mm gap has a weaker electric field close to the exposed electrode but the electric field decays much more slowly. It was expected that actuators with overlapping electrodes would produce more thrust at higher pressure where the plasma is formed where the electric field is stronger while the actuator with a gap would produce more thrust at low pressures where the plasma extends farther downstream. Figure 1.14, shows that for an actuator with $b = 15$ mm the maximum thrust production with $c = 3$ mm occurs at 50 kPa whereas when $c = -3$ mm the maximum thrust production occurred at 60 kPa. Regardless, the actuator with $c = 1$ mm outperformed the other actuators at all pressures. However, this trend appears to be reversed in Figure 1.16 where for $b = 75$ mm the $c = -3$ actuator produced more thrust at low pressure than the $c = 3$ mm actuator. Again the $c = 1$ mm actuator produced the most thrust at all pressures.

Figure 1.15 shows that the $b = 15$ mm and $c = 3$ mm plasma actuator is significantly more effective at 70 kPa and above than the $c = 1$ and -3 mm designs. This is possibly due to the increased directionality of the electric field not shown in Figure 1.21. While the magnitude of the electric field decreases near the edge of the exposed electrode due to the increased separation between the exposed and buried electrodes the component of the electric field in the downstream direction does not decrease as much as the component normal to the dielectric. This increased directionality could be more effectively accelerating the plasma downstream. However, the $b = 75$ mm actuator did not exhibit an increase in effectiveness as gap length is increased as seen in Figure 1.17.

1.5. CONCLUSION

Low pressure performance of SDBD plasma actuators was investigated at pressures ranging from 10-101 kPa. The effects of buried, and exposed electrode length, as well as chord-wise gap, on actuator thrust production and effectiveness were studied. As buried electrode length is increased, the electric field extends farther downstream, and thrust production at high pressure initially decreases, but increases at low pressure. However, as buried electrode length is increased further, thrust production increases at all pressures. Altering the length of the exposed electrode and chord-wise gap does not have as large of an effect on thrust production except at high pressures where actuators with $a = 15$ mm and $c = 1$ mm produced the most thrust. While altering the exposed electrode length and chord-wise gap did not improve thrust production increasing the chord-wise gap did improve actuator effectiveness. At 70 kPa and above an actuator with $a = 15$ mm, $b = 15$ mm, and $c = 3$ mm was on average 22% more effective than the original design of $c = 1$ mm. All the actuators studied in this experiment exhibited a nearly linear relationship between effectiveness and operating pressure. The most effective actuator studied had a buried electrode of 50 mm and exposed electrode of 15 mm with a 1 mm gap, on average

over all pressures it was 14% more effective than the baseline $b = 15$ mm design. The actuator which produced the most thrust overall had a buried electrode length of $b = 75$ mm. This design produced 26% more thrust at all pressures than the baseline $b = 15$ mm design and produced 34% more thrust between the pressures of $20 - 40$ kPa. Plasma actuators with long chord-wise buried electrode lengths will offer more aerodynamic control thrust to aircraft in low pressure environments.

2. PLASMONIC FORCE PROPULSION (PFP) THRUSTERS

2.1. INTRODUCTION

Low mass cube satellites or cubeSats are growing in popularity with NASA, the DoD, and student design teams at universities, because of their low cost, versatility, and the ease of being incorporated with other space launches.[24, 25] Most cubeSats are a 10x10x10 cm cube or a combination of 10x10x10 cm cube units. Because of the mass and volume constraints on cubeSats, incorporating propulsion and Attitude Control Systems (ACS) small enough to fit onto cubeSats while still retaining enough mass/volume for instruments is quite challenging. The majority of cubeSat propulsion and Reaction Control Systems (RCS) are low thrust but high specific impulse electric/plasma thrusters which require high voltage and power. Because of the additional hardware required to power these systems incorporating them onto a cubeSat leaves little room for payload.

Plasmonic Force Propulsion (PFP) thrusters use the interaction between focused sunlight and sub-wavelength nanostructures to accelerate nanoparticles. The thrusters are approximately the size of a human hair, require no power, and have negligible mass compared to the rest of the spacecraft systems. The only mass and volume requirements come from the propellant, propellant tanks, and a focusing lens. It is estimated that the thrusters will have low thrust (10-500 nN) and low specific impulse (1-12 s). The low thrust and high switching time of PFP thrusters makes them ideal for spacecraft which require extremely high precision pointing or positioning. The simulations presented in this study estimate that a 1U 2 kg cubeSat employing PFP thrusters could maintain a pointing accuracy of ~1×10^{-9} degrees or ~4×10^{-3} milliarcseconds and a positioning accuracy of 10 pm!

This analysis is the third part of a three part study on PFP thrusters funded by the NASA Innovative Advanced Concepts (NIAC) program. Research on all three parts were

carried out simultaneously by different students at the Missouri University of Science and Technology under the direction of Dr. Joshua Rovey and Dr. Xiaodong Yang. The first part of the study was to characterize the interaction between light and the nanostructures to determine the plasmonic force between an individual structure and individual particle. This study was conducted by Changyu Hu under the direction of Dr. Yang. The second part of the study was to determine the thrust and specific impulse of a thruster made up of an array of the previously mentioned nanostructures. The second study was conducted by Matthew Glascock under the direction of Dr. Rovey. The third study is detailed in this document and analyzes the performance characteristics of PFP thrusters when used by cubeSats. This document provides a comparative analysis of several different cubeSat propulsion and RCSs. Primarily the document looks at the pointing accuracy of the thruster systems when used as an ACS and the proximity control capabilities of the thrusters when used as a RCS for formation flying. A summary of all of the results of this study can be seen in Table 2.1. The algorithms used to determine the pointing and positioning accuracy are described in Section 2.2. A detailed description of PFP thrusters, how they work, their capabilities, and how they compare with different cubeSat RCSs is found in Section 2.3, and a discussion of current problems with PFP thrusters and potential solutions is presented in Section 2.4.

2.2. CUBESAT CONTROL SIMULATIONS

Three separate programs were written in MATLAB to simulate three different control scenarios; attitude control using RCS thrusters, proximity control using RCS thrusters, and attitude control using reaction wheels. Each of these scenarios involve the cubeSat employing a "Bang Bang" or "On/Off" control algorithm to move to or maintain a desired position or attitude in the presence of Solar Radiation Pressure (SRP). Section 2.2.1 provides a qualitative description of Bang Bang control algorithms, and Section 2.2.2 gives a qualita-

tive description of how they are employed in the three simulations. Section 2.2.3 describes how the solar radiation pressure was modeled. Finally, Sections 2.2.5, 2.2.4, and 2.2.6 provide a detailed mathematical description of the programs used to simulate attitude control with RCS thrusters, proximity control using RCS thrusters, and attitude control using reaction wheels respectively.

2.2.1. Qualitative Description of Bang-Bang Control Algorithms. A bang-bang or on/off control algorithm is an algorithm which differs from conventional controllers in that it has only two settings: on at maximum power and off at zero power. Traditional control algorithms usually involve a range of power levels.

As an example, consider the familiar control system of an automobile. There are the gas pedal and break pedal which control acceleration and deceleration, and the steering wheel which controls the cars "attitude" or the direction it is pointing. Each of these controllers can be set at a range of values. If the driver wishes to accelerate to a speed of 70 mph he will press the accelerator down until the car reaches 70 mph. If he wishes to accelerate faster or slower he can apply more or less pressure to the pedal, which in turn supplies a greater or lesser amount of gas to the engine. As the car approaches 70 mph he can slowly remove pressure from the accelerator until just the right amount of gas is being supplied to the engine to counteract the friction and wind resistance which is slowing the car down.

Now consider a car with a *bang-bang* control system where the gas and break pedals can either be pressed all the way down or not at all and the steering wheel can only be turned all the way to the right, all the way to the left, or centered. This is called a bang-bang control algorithm because if the car is below the desired speed, *bang!*, the engine turns on accelerating the car. When the desired speed is reached, *bang!* the engine turns off again. Accelerating to 70 mph would be quite violent, and take a matter of seconds. Once at 70 mph the engine would turn off. Gradually the car would decelerate because of friction and if the driver took no action eventually the car would come to a stop. In order

to maintain an average speed of 70 mph the driver will have to accelerate to a speed above the desired average speed say 75 mph and then wait for the car to decelerate to a speed below the that which is desired, say 65 mph before applying the gas again. This acceptable range of values around the desired speed is known as the *switching interval*. By turning the engine on and off faster a narrower switching interval can be achieved. If the engine was able to turn on and off instantaneously then the speed could be maintained exactly at 70 mph! However, engines cannot be turned on and off instantaneously they require a characteristic start up time known as the *switching time*. Thus the minimum size of the switching interval around the desired speed is determined by three factors, the switching time of the engine, the amount of force the engine provides when it is on, and the strength of the disturbing forces.

The same rules apply to the reaction control thrusters on-board spacecraft as the fictional engine of the car which can only be on or off. Instead of maintaining a desired speed, the spacecraft is maintaining a desired position and/or attitude with a switching interval given in either meters or degrees. Some reaction control thrusters are throttleable, but many are not, also throttleable reaction control thrusters are usually only operated at one optimal level and used in an on/off configuration.

The bang-bang algorithms used in this study are more complicated than the simple example presented above. The algorithms used here make decisions about when to turn the thrusters on or off based on the current error in position or attitude. They also factor in the rate at which the error is changing. This is called a Proportional Derivative or PD controller because it keeps track of both the error and the derivative of the error with respect to time.[1] The addition of the differential term allows the spacecraft to avoid overshooting the bounds of the switching interval.[26, 27]

[1]Note: Since only one thrust level is allowed this is not technically a PD controller because the amount of thrust applied by the thrusters is not truly *proportional* to the magnitude of the error. However, many authors such as Fortescue still refer to these as PD controllers[26]

2.2.2. Qualitative Description of Implementation of Bang-Bang Control Algorithms. The codes for the attitude and position control simulations presented in this study was written in MATLAB and the algorithms are as follows. The user inputs mass and size of a cubeSat, as well as the thruster moment arm, thrust, number of thrusters, specific impulse, and the switching time of the thruster to be tested. The *worst case scenario* solar radiation torque or force is calculated using the cubeSat size as described in Section 2.2.3. The user then defines an initial attitude/position, initial velocity, a desired attitude/position, and switching interval.

The body of the code is a "for" loop where each iteration calculates the satellite current position or attitude, and is illustrated by the flow chart in Figure 2.1. In each iteration the thruster is either on or off for the switching time of the thruster. The simulation keeps track of the spacecraft attitude/position and velocity, and decides whether or not it is necessary to fire the thruster and in which direction the thruster should be fired to keep the satellite at the desired attitude/position. It is assumed that the satellite sensors measure the attitude/position and the angular velocity/linear velocity with zero error. If the current attitude/position is outside of the switching interval then the spacecraft fires its thrusters in the appropriate direction to arrive at the set attitude/position. The spacecraft constantly calculates the distance it will take to stop if it decelerated constantly from its current velocity to zero. When that distance equals the distance away from the set attitude/position the spacecraft will decelerate to zero velocity. If the attitude/position is inside the switching interval the spacecraft measures its velocity. If the velocity is greater than the smallest change in velocity the thrusters are capable of producing and the velocity and pointing error are both positive or both negative (meaning the attitude vector is moving away from the desired attitude) then the thrusters will fire in order to nudge the spacecraft back toward the desired position/attitude.

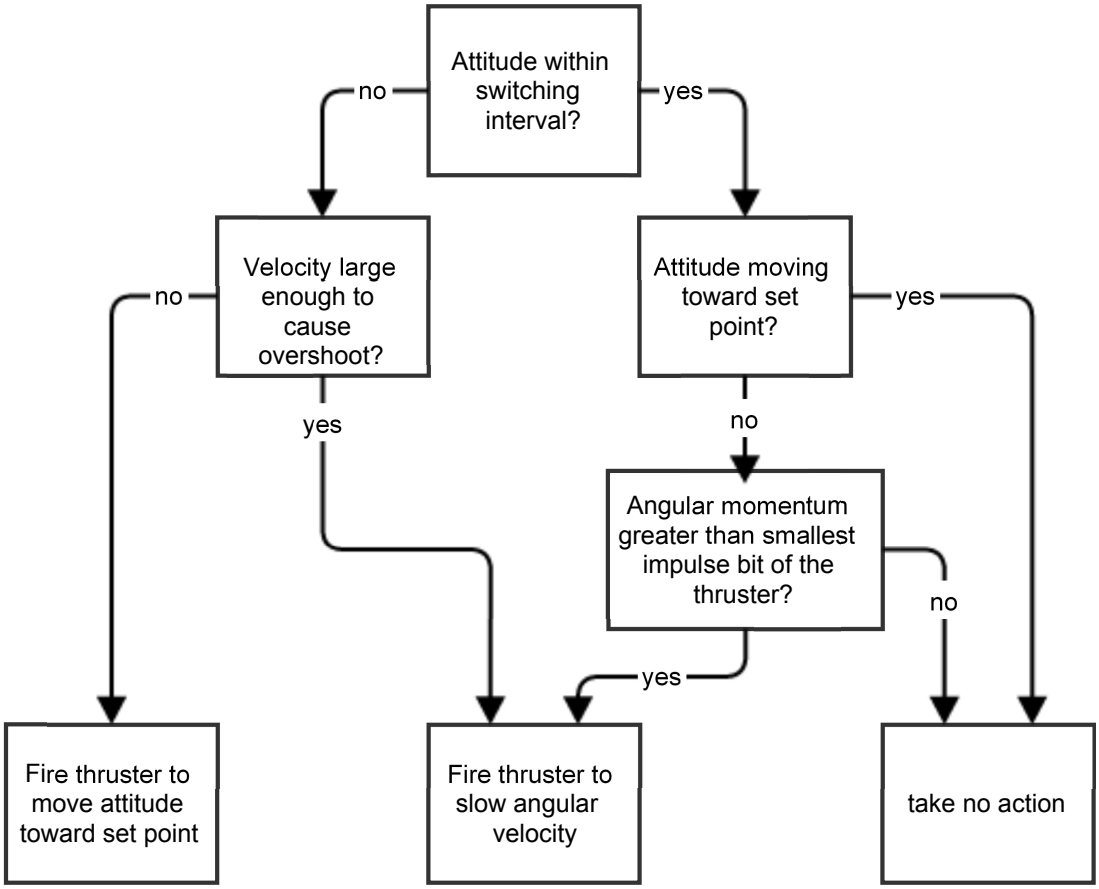

Figure 2.1: Flow chart outlining the PD bang-bang control algorithm used for attitude control.

The same flow chart can used for proximity control by simply replacing the words *attitude*, *angular momentum,* and *angular velocity* with *position*, *momentum*, and *velocity* respectively.

Throughout the simulation the current attitude/position, velocity, torque/force, and propellant consumption are recorded and plotted. If the thruster is not capable of keeping the attitude/position of the satellite within 10% of the switching interval a warning will be displayed stating that the current thruster is not capable of maintaining the switching interval desired.

2.2.3. Modeling Solar Radiation Pressure (SRP). In space there are a number of forces which can perturb the attitude and orbit of a spacecraft. If the spacecraft is suf-

ficiently long then the end closer to the earth will experience a greater gravitational force then the end farther away causing a tidal torque. Similarly the earths magnetic field can exert tiny torques on a spacecraft changing its attitude. A large mountain range or other geographic feature may alter the earths local gravitational field changing the spacecraft orbit. Also, in low earth orbit there are still some remnants of the earths atmosphere which exert a slight aerodynamic drag. However, above 400 km the largest disturbing on a spacecrafts attitude is solar radiation pressure (SRP).[27] SRP is also one of the largest disturbing forces on satellites formation flying while in the same orbit.

SRP is the force from sunlight striking the surface of a spacecraft. All electromagnetic radiation carries momentum related to its energy and thus its wavelength. The momentum carried by a single photon is given by equation 2.1

$$p = \frac{h}{\lambda} \tag{2.1}$$

Where p is the magnitude of the momentum, h is Plank's constant and λ is the wavelength of the photon. The direction of the momentum vector is the same as the direction of the photon propagation.[28] Note that if a photon is absorbed by a surface the momentum transfered will be equal to p but if it is reflected back the way it came the momentum transfer will be $2p$. Given that $h = 6.626 \times 10^{-34}$ J·s the amount of momentum carried by a single photon is very small. However, in space, where there are very few outside forces, the SRP is able to push satellites off course or produce a torque on a spacecraft causing its attitude to drift. In fact, SRP is the primary external torque on satellites in orbits above 400 km, below which, aerodynamic torques dominate.[27].

The SRP or mean momentum flux, P, acting on a flat surface normal to the Sun's incident rays is given by

$$P = \frac{F_e}{c} \tag{2.2}$$

where F_e is the intensity of the Sun's light known as the solar constant given in $\frac{W}{m^2}$ and c is the speed of light. The intensity of any electromagnetic wave is given by taking the time average of the waves Poynting vector, **S**, given by

$$\mathbf{S} = \frac{1}{\mu_0}(\mathbf{E} \times \mathbf{B}) \tag{2.3}$$

where μ_0 is the permeability of free space, and **E** and **B** are the waves oscillating electric and magnetic field vectors. Thus the time averaged intensity, I, is given by

$$I = \frac{1}{T}\left| \int_0^T \mathbf{S} dt \right| \tag{2.4}$$

[29] In the case of light from the Sun at 1 AU $I = F_e = 1358\ \frac{W}{m^2}$. However, because of the eccentricity of the Earth's orbit F_e varies between 1314 $\frac{W}{m^2}$ and 1404 $\frac{W}{m^2}$. The solar constant actually varies according to

$$F_e = \frac{1358}{1.0004 + 0.0334\cos(D)}\ \frac{W}{m^2} \tag{2.5}$$

where D is the "phase" of the year measured from July 4 when the earth is at its furthest point from the Sun or aphelion. However, for the purpose of this model the solar constant will be taken as its average value of $F_e = 1358\ \frac{W}{m^2}$.[27, 30]

There are three ways in which momentum can be transfered from incident radiation to a rigid body: absorption, specular reflection, and diffuse reflection. Absorption is where incident photons are absorbed by the material transferring their energy to heat and their momentum to the surface, as happens when light shines on a black piece of paper or other black object. The differential radiation force on an elemental area dA is given by

$$d\mathbf{f}_{absorbed} = -PC_a \cos(\theta)\hat{\mathbf{S}} dA \qquad (0 \leq \theta \leq 90^\circ) \tag{2.6}$$

where $\hat{\mathbf{S}}$ is the unit vector from the surface to the Sun (*i.e.* the opposite direction of photon propagation), C_a is the absorption coefficient (*i.e.* the fraction of light which is absorbed), θ is the angle between $\hat{\mathbf{S}}$, and $\hat{\mathbf{N}}$, the unit outward normal from the elemental area dA. If θ is negative then the surface is not illuminated and thus will experience no force.[27, 28, 30]

Specular reflection is when the incident lights reflected angle relative to $\hat{\mathbf{N}}$ is equal to its incident angle θ. In common English this just means that the light is reflected by a mirrored surface, such as a shiny piece of metal, or the surface of a pane of glass. The differential radiation force due to specular reflection is

$$d\mathbf{f}_{specular} = -PC_s \cos^2(\theta)\hat{\mathbf{N}}dA \qquad (0 \leq \theta \leq 90^\circ) \tag{2.7}$$

where C_s is the coefficient of specular reflection which is the fraction of incident light which is reflected specularly. [27, 28, 30]

Finally, the third form of momentum transfer from radiation is diffuse reflection, which is where incident light is reflected in all directions away from the surface. This is the type of reflection observed when shining a light on a white piece of paper or another white surface. Diffuse reflection is the type of reflection which allows us to see everyday objects around us such as desks, chairs, vacuum chambers, and ion drives. The differential force for radiation which has been diffusely reflected is given by

$$d\mathbf{f}_{diffuse} = -PC_d\left[-\frac{2}{3}\cos(\theta)\hat{\mathbf{N}} - \cos(\theta)\hat{\mathbf{S}}\right]dA \qquad (0 \leq \theta \leq 90^\circ) \tag{2.8}$$

where C_d is the coefficient of diffuse reflection or the faction of the incident radiation which is diffusely reflected.[27, 28, 30]

Assuming that no light is transmitted by the surface then $C_a + C_s + C_d = 1$. Thus the total differential radiation force is given by

$$d\mathbf{f}_{total} = d\mathbf{f}_{absorbed} + d\mathbf{f}_{specular} + d\mathbf{f}_{diffuse} \tag{2.9}$$

where

$$d\mathbf{f}_{total} = -P\left[\left(1 - C_s\right)\hat{\mathbf{S}} + 2\left(C_s\cos(\theta) + \frac{1}{3}C_d\right)\hat{\mathbf{N}}\right]\cos(\theta)dA \tag{2.10}$$

Thus the total force, $\mathbf{F}$, on the surface due to SRP is given by,

$$\mathbf{F} = \int d\mathbf{f}_{total} \tag{2.11}$$

and the torque due to SRP, τ_{solar}, on a surface is given by,

$$\tau_{solar} = \int \mathbf{R} \times d\mathbf{f}_{total} \tag{2.12}$$

where $\mathbf{R}$ is the vector from the spacecrafts center of mass to the elemental area dA.[27, 30]

Now integrating Eq 2.10 over a plane of surface area A, such that $\theta = \cos^{-1}\left(\hat{\mathbf{S}} \cdot \hat{\mathbf{N}}\right)$ the force on such a flat plate is given by

$$\mathbf{F}_{total} = -PA\cos(\theta)\left[\left(1 - C_s\right)\hat{\mathbf{S}} + 2\left(C_s\cos(\theta) + \frac{1}{3}C_d\right)\hat{\mathbf{N}}\right] \tag{2.13}$$

Integrating Eqs 2.11 and 2.12 over all the surfaces of a spacecraft would give exact values for the solar force and torque disturbing the desired motion of the spacecraft. However, doing so is complicated and is not useful for the analysis in this study. It is common practice when comparing the performance of various reaction control and attitude control systems to simply use the "worst case scenario" disturbance forces and torques.[31] For a 1U cubeSat the worst case scenario solar radiation disturbance force is when one face of

the cubeSat is directly facing the Sun such that $\hat{\mathbf{S}} \cdot \hat{\mathbf{N}} = 1$ then $\cos^{-1}\left(\hat{\mathbf{S}} \cdot \hat{\mathbf{N}}\right) = \theta = 0$ and all the light is reflected specularly (*i.e.* $C_a = C_d = 0$ and $C_s = 1$). Then Eq 2.13 becomes

$$\mathbf{F}_{total} = -2PA\hat{\mathbf{N}} \tag{2.14}$$

For a 1U cubeSat with $A = 100$ cm^2 the force given by Eq 2.14 is $F = 90.6 \times 10^{-9}$ N. This is the value of solar radiation force which was used in the proximity control using reaction control thrusters simulations outlined in Section 2.2.4.

There are many possible ways to determine a "worst case scenario" solar radiation torque. One which readily comes to mind is the poor design decision of making one half of a face of the cubeSat mirrored and the other half painted black so that it absorbs all incident light. In the case where that face is directly facing the Sun (*i.e.* $\theta = 0$) the force on the reflective half of the face will be twice that on the absorbent face, producing a torque of magnitude $\tau = \frac{1}{8}PAL$ where L is the length of one side of the cubeSat (note that the moment arm in this case is L/4). This is not truly the worst case scenario though. The true worst case scenario would be where one face of the cubeSat is completely reflective and directly facing the Sun and half of that face is shaded by a neighboring satellite or space station. In such a situation the magnitude of solar radiation torque would be

$$\tau = \frac{1}{4}PAL. \tag{2.15}$$

Assuming a 1U cubeSat with $L = 10$ cm, and $A = 100$ cm^2, $\tau = 1.13 \times 10^{-9}$ N·m. This scenario may seem far-fetched but NASA and other organizations are looking into the feasibility of missions involving vast arrays of cubeSats flying in formation.[32, 33] In such a mission it would be common place for cubeSats to be moving in and out of each others shadow, or spend appreciable amounts of time partially shaded. Eq 2.15 gives the value of solar radiation torque which is used in the models presented in Sections 2.2.5 and 2.2.6

2.2.4. Proximity Control Using Reaction Control Thrusters. This section describes in detail the mathematical model used to model position control using RCS thrusters. The MATLAB code implementing this model may be viewed in Appendix A. The assumptions of this model are as follows:

1. There are no outside forces affecting the motion of the spacecraft other than its thrusters and solar radiation pressure.
2. This is a single axis simulation so all forces (thrust and SRP) act only along that axis.
3. The spacecraft always knows its current position and velocity with perfect accuracy.
4. The point/object/other satellite which the spacecraft is trying to maintain proximity to is inertially fixed.
5. SRP is constant and is calculated for the *worst case scenario* where the Sun is directly behind the spacecraft and the spacecraft surfaces reflect light perfectly back toward the Sun.
6. The attitude of the spacecraft remains constant such that one face of the cubeSat is directly facing the Sun.
7. The spacecraft is a cube with constant density.
8. For every time step of the simulation the thrusters can either be fired or not fired. There is no *recharge time* for the thrusters and each burst delivers the exact same impulse bit for the specified switching time.
9. Because fuel consumed during simulations is very small (usually less than 1 mg) the spacecraft is assumed to have constant mass.

Spacecraft inputs are its mass, M in kg, and the length of a side of the cubeSat, L in m. Thruster inputs are thrust, F in N, switching time, t in s, specific impulse, I_{sp} in s,

number of thrusters, n, and the mass of on board propellant, M_p in kg. From these values important performance characteristics can be calculated such as *impulse bit*, I_b, and *delta V*, ΔV. *impulse bit* is the minimum amount which a thruster is capable of changing the momentum of the spacecraft when it fires for the minimum amount of time allowed by the switching time and is given by

$$I_b = Ft. \tag{2.16}$$

Delta V is the total amount which the spacecraft is capable of changing its velocity and is given by the famous Tsiolkovsky rocket equation

$$\Delta V = V_{exit} \ln\left[\frac{M}{M - M_p}\right] \tag{2.17}$$

where V_{exit} is the exit velocity of the exhaust leaving the thruster. $V_{exit} = gI_{sp}$ where g is the mean standard acceleration due to gravity on Earth's surface.[2] It is clear from Eq 2.17 that there are two way to increase the total ΔV of a spacecraft, by increasing the mass of propellant on board and by increasing the thruster I_{sp}. In Section 2.3 it will be shown that PFP thrusters small mass and volume allow for easy incorporation on a spacecraft but their low I_{sp} requires greater amounts of propellant.

Next values relevant to the simulation are calculated. The spacecraft is assumed to be under constant acceleration from SRP given by Eq 2.14 in Section 2.2.3. Only now it is assumed that $\hat{\mathbf{N}} = -\hat{\mathbf{x}}$ so Eq 2.14 becomes

$$\mathbf{F}_{SRP} = 2PA\hat{\mathbf{x}} \tag{2.18}$$

[2] $g = 9.8$ m/s^2 *always*. Thruster efficiencies are measured in terms of specific impulse instead of exit velocity for historical reasons which are not relevant to this thesis.

For a 1U cubeSat with one face directly facing the Sun $\mathbf{F}_{SRP} = 90.6$ nN. Thus the acceleration of the cubeSat from SRP is

$$\mathbf{a}_{SRP} = \frac{\mathbf{F}_{SRP}}{M} \tag{2.19}$$

If the thrusters are fired then they will produce an acceleration as well given by

$$\mathbf{a}_{thrust} = \frac{n\mathbf{F}}{M} \tag{2.20}$$

where n is the number of thrusters firing and $\mathbf{F}$ is the thrust of each thruster.

Next after initializing the position, velocity and desired position the simulation begins. Each iteration represents a time step lasting for the switching time t. During each iteration the bang-bang algorithm described in Section 2.2.2 decides whether to fire the thrusters in the $+\hat{\mathbf{x}}$ direction or the $-\hat{\mathbf{x}}$ or to take no action. Also, each iteration the distance required for the spacecraft to stop at its current velocity is calculated using the basic kinematic equations found in any elementary physics text.[34, 35]

$$x_{stop} = \frac{1}{2}\frac{V^2}{a_{thrust}} \tag{2.21}$$

In the case where the spacecraft is outside of the switching interval but moving toward the desired position this number is used to decide whether the thrusters should continue firing toward the desired position or fire the opposite direction bringing the spacecraft to a stop. After deciding whether or not to fire the thrusters and in what direction the current position and velocity of the spacecraft is updated.

$$x_{new} = x_{old} + \frac{1}{2}a_{thrust}t^2 + \frac{1}{2}a_{SRP}t^2 + V_{old}t \tag{2.22}$$

$$v_{new} = v_{old} + a_{thrust}t + a_{SRP}t \tag{2.23}$$

Where $a_{thrust} = \pm\frac{nF}{M}$ or 0 depending on whether or not the thrusters are being fired and in which direction. Finally the total time the thrusters have been operating,T is recorded and the mass of propellant which has been expended, M_e is calculated using[36]

$$M_e = \frac{nFT}{gI_{sp}}. \tag{2.24}$$

Plots of the spacecraft's position and velocity, as well as the force produced by the thrusters, the error in the position and velocity, and the propellant consumed are produced. A sample output of the simulation is provided in Figure 2.2. The sample output shown in Figure 2.2 was simulating a 2 kg 1U cubeSat with two PFP thrusters producing 250 nN of thrust with a switching time of 1 ms. The cubeSat moved 1×10^{-10} m then held position within a switching interval of 2×10^{-12} m all while under a 90 nN disturbance force from SRP.

Limitations of RCS model. At this point the assumption of knowing position and velocity to perfect accuracy begins to break down. The most accurate laser interferometers can only measure lengths to within a fraction of a wavelength of light.[28] Interferometers exist which can measure sub-angstrom lengths but they aren't the sort of instruments which would easily fit on a cubeSat.[37, 38] However, the purpose of the simulation is not to determine the actual positioning accuracies, but the theoretical limits of positioning accuracy.

While it may not be possible for cubeSats to fly with such precision NASA is currently developing the technology to allow the three spacecraft of the Laser Interferometer Space Antenna or LISA mission to be able to detect their position relative to each other with picometer precision. The mission of LISA is to detect and pinpoint sources of gravitational waves in space. In order to do this the LISA spacecraft must be able to detect changes in the distance between each spacecraft on the order of tens of picometers over 5,000,000 km! The requirements for the thrusters currently being developed for these spacecraft is that

they have a thrust of 5-30 μN.[15–17] An array of tens of PFP thrusters would be able to produce thrusts on that level making PFP thrusters a possible option for the LISA mission. While a single PFP thruster producing thrusts on the level of 50-500 nN could allow for even higher positioning accuracies on future NASA missions.

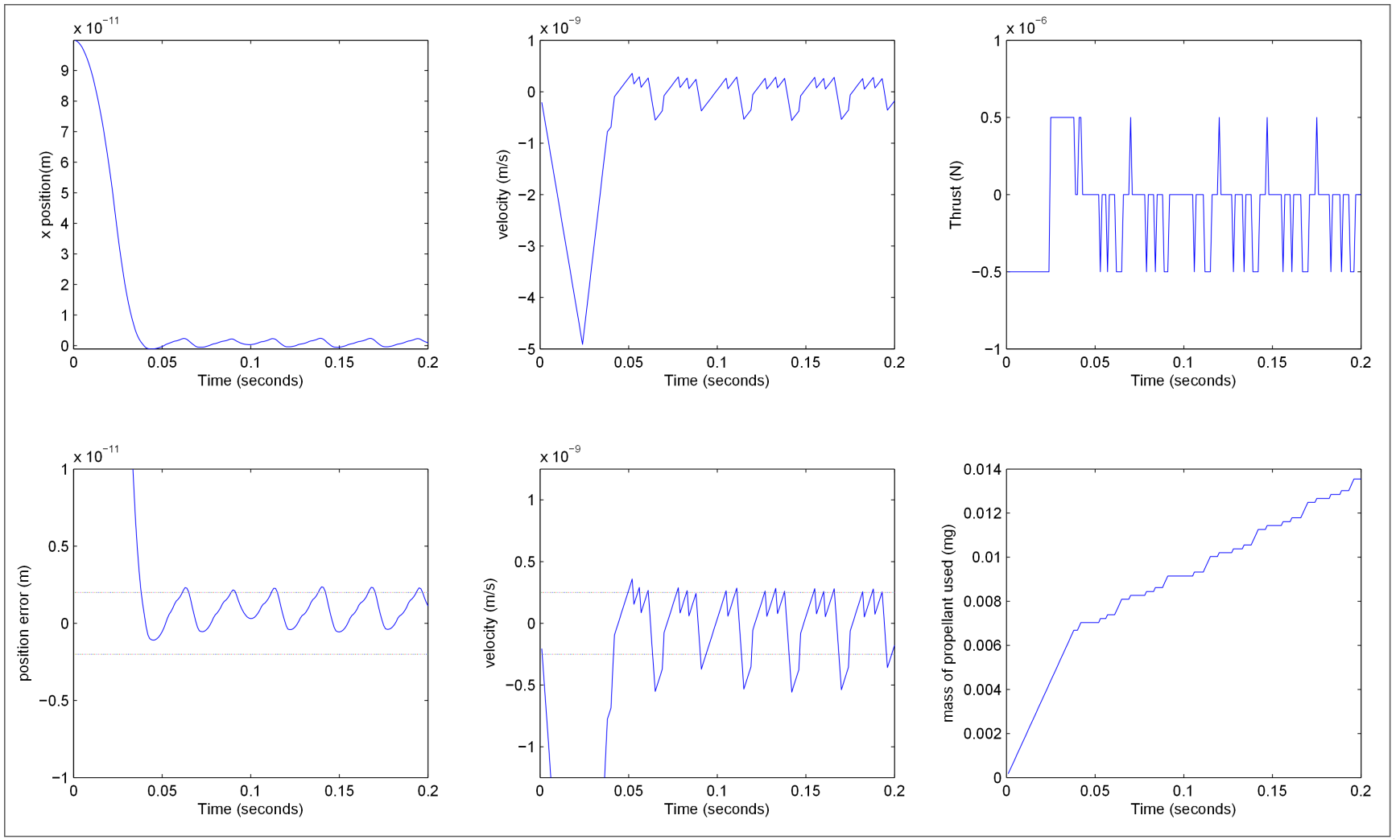

Figure 2.2: Sample output of proximity control simulation.

2.2.5. Attitude Control Using Reaction Control Thrusters. This section describes in detail the mathematical model used to model attitude control using RCS thrusters. The MATLAB code implementing this model may be viewed in Appendix B. The assumptions of this model are as follows:

1. There are no outside forces affecting the rotation of the spacecraft other than its thrusters and torque from solar radiation pressure.

2. This is a single axis simulation so all torques (thrust and SRP) act only along that axis of rotation.

3. The spacecraft always knows its current angular position and angular velocity with perfect accuracy.

4. Solar radiation torque is constant and is calculated for the *worst case scenario* where the Sun is directly behind the spacecraft, and half of the surface facing the Sun reflects its light perfectly and the other half is shaded.

5. All attitude changes are small such that the torque from SRP remains constant

6. The spacecraft is a cube with constant density.

7. For every time step of the simulation the thrusters can either be fired or not fired. There is no *recharge time* for the thrusters and each burst delivers the exact same impulse bit for the specified switching time.

8. Because fuel consumed during simulations is very small (usually less than 1 mg) the spacecraft is assumed to have constant mass.

Spacecraft inputs are its mass, M in kilograms, and the length of a side of the cubeSat, L in meters. Thruster inputs are thrust, F in Newtons, switching time, t in seconds, specific impulse, I_{sp} in seconds, number of thrusters, n, and the moment arm of the thrusters

$r = L/2$ in meters. For attitude control using RCS thrusters at least two thrusters must fire simultaneously on both sides of the spacecraft to prevent any translation.

Next the physical characteristics of the spacecraft, or the *plant* of the control system are calculated. Since the cubeSat is assumed to be a cube of constant density its moment of inertia is give by [34, 35]

$$J_{sat} = \frac{1}{6}ML^2. \tag{2.25}$$

The torque produced by the thrusters when they are firing is given by [34, 35]

$$\tau_{thrust} = nrF \tag{2.26}$$

Thus the angular acceleration of the spacecraft when the thrusters are firing is given by

$$\alpha_{thrust} = \frac{\tau_{thrust}}{J_{sat}} \tag{2.27}$$

Next the *worst case scenario* disturbance torque from solar radiation pressure is calculated from Eq 2.15

$$\tau_{solar} = \frac{1}{4}PAL. \tag{2.15}$$

Eq 2.15 evaluated for a 1U cubeSat with $L = 10$ cm, and $A = 100$ cm^2, gives $\tau = 1.13 \times 10^{-9}$ N·m. Thus the angular acceleration due to SRP is

$$\alpha_{solar} = \frac{\tau_{solar}}{J_{sat}} \tag{2.28}$$

With all of the preliminary calculations done the attitude control simulation begins as described in Section 2.2.1. Each iteration again represents one time step equal to the switching time of the thruster system. The angular distance required to stop the spacecraft rotation at

its current angular velocity is calculated every iteration using

$$\theta_{stop} = \frac{1}{2}\frac{\omega^2}{a_{thrust}} \tag{2.29}$$

where ω is the cubeSats current angular velocity. In the case where the spacecrafts attitude is outside of the switching interval but moving toward the desired attitude this number is used to decide whether the thrusters should continue firing toward the desired position or fire the opposite direction bringing the spacecrafts rotation to a stop. After deciding whether or not to fire the thrusters and in what direction the current attitude and angular velocity of the spacecraft are updated.

$$\theta_{new} = \theta_{old} + \frac{1}{2}\alpha_{thrust}t^2 + \frac{1}{2}\alpha_{solar}t^2 + \omega_{old}t \tag{2.30}$$

$$\omega_{new} = \omega_{old} + \alpha_{thrust}t + \alpha_{solar}t \tag{2.31}$$

Where θ is the spacecrafts attitude, ω is its angular velocity, and t is the switching time of the thruster. $\alpha_{thrust} = \pm\frac{nF}{M}$ or 0 depending on whether or not the thrusters are being fired and in which direction. Finally the total time the thrusters have been operating, T is recorded and the mass of propellant which has been expended, M_e is calculated using[36]

$$M_e = \frac{nFT}{gI_{sp}}. \tag{2.24}$$

A sample output of the attitude control simulation is shown in Figure 2.3, showing how the spacecrafts attitude, and angular velocity vary with time as well as when the thrusters fire and the propellant usage. The simulation shown in Figure 2.3 was for two PFP thrusters mounted on either side of a 2 kg 1U cubeSat scaled such that their thrust was only 50 nN. The thrusters also had a specific impulse of 2.9 s, and a switching time of 1 ms. The cubeSat rotated a distance of 5×10^{-8} degrees which is 1.8×10^{-4} arc-seconds then

came to a stop and maintained a switching interval of 1×10^{-9} degrees or 3.6×10^{-6} arcseconds in the presence of SRP. The solar radiation torque was pushing the cubeSat in the $+\hat{\theta}$ direction which is what caused it to overshoot as it approached the set attitude of zero degrees.

Limitation of ACS model. While the thruster may be theoretically capable of maintaining a switching interval of 1×10^{-9} due to the relative strength of the thruster torque, and solar radiation pressure torque the assumption of knowing angular position to perfect accuracy breaks down. Assuming the cubeSat was using some sort of optical telescope mounted on it for attitude sensing it would not even be able to sense the 5×10^{-8} degree attitude change shown in Figure 2.3 because of diffraction. Because of the wave nature of light, diffraction limits the angular resolution of any optical instrument. The smallest angle which can be resolved by an optical instrument is given by

$$\phi_d = \sin^{-1}\left(1.22\frac{\lambda}{a}\right) \tag{2.32}$$

where ϕ_d is the diffraction limited angle λ is the wavelength of light observed and a is the diameter of the aperture of the optical instrument.[28, 39] Thus even if the cubeSat was fitted with a diffraction limited $a = 10$ cm diameter ultraviolet telescope sensing light with wavelengths of $\lambda = 1$ nm the best angular resolution achievable by that telescope would be $\phi_d = 7 \times 10^{-7}$ degrees! Even so, if PFP thrusters were to be employed on a cubeSat or larger satellite such as a space telescope they would be able to provide a pointing accuracy which was limited by the spacecraft attitude sensing instruments not by the attitude control thrusters.

One proposed NASA mission which requires an extremely high pointing precision of 0.1 milliarcseconds is The Stellar Imager. This space based ultraviolet telescope will have over 200$\times$ the resolution of the Hubble Space Telescope and will be able to take images showing details on the surfaces of other stars. The Stellar Imager will consist of

20-30 small "mirror sats" flying in formation to produce a giant mirror. To to this each "mirror sat" will need to be placed with nanometer precision and control its attitude with milliarcsecond precision. The mission concept is still under development, but it is clear that The Stellar Imager will need extremely fine pointing capabilities which could be provided by enabling technologies such as PFP thrusters.[18–20]

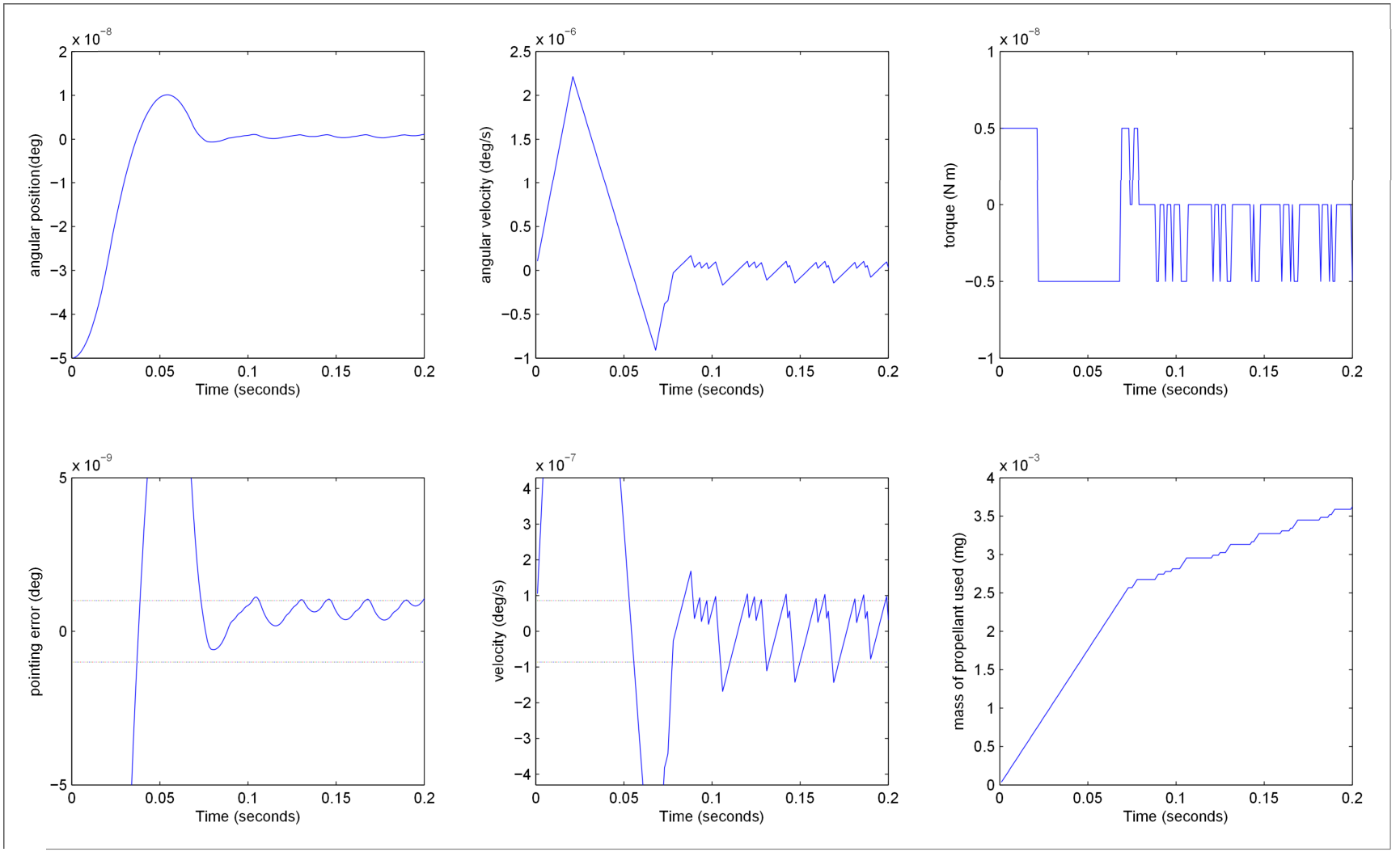

Figure 2.3: Sample output of attitude control simulation.

2.2.6. Attitude Control Using Reaction Wheels. Reaction wheels are an attitude control mechanism which use the law of conservation of angular momentum to control the rotation of a satellite. A reaction wheel is simply a fly wheel which has its angular velocity constantly controlled by an electric motor. Since the angular momentum of the satellite–reaction wheel system is conserved, when the motor produces a torque on the reaction wheel a counter torque equal in magnitude and in the opposite direction is applied to the satellite. The primary characteristics of reaction wheels which determine its pointing accuracy are its moment of inertia, and the precision with which it can maintain a certain rotation rate.[26, 27, 40, 41]

Since reaction wheels have variable torque generally models of control systems use a Proportional Integral Derivative or PID feedback control model. However, such models, while excellent for controlling attitude maneuvers, will yield the non physical result of zero steady state pointing error.[41, 42] Because of this a model almost identical to the *bang bang* control model used in Section 2.2.5 will be used. In this model the reaction wheel will be operated in *minimum torque mode*. As the name implies in this mode there will be one magnitude of torque on the reaction wheel which corresponds to the minimum amount the reaction wheels angular velocity can be changed. As a result this model will not be useful for determining the minimum time it takes for the spacecraft to perform a certain maneuver. Rather this model determines the minimum pointing error possible for a particular reaction wheel.

The MATLAB code for this model is available in Appendix C. The assumptions of this model are as follows:

1. There are no outside forces affecting the rotation of the spacecraft other than the torque from the reaction wheel and torque from solar radiation pressure.

2. This is a single axis simulation so all torques (from the reaction wheel and SRP) act only along that axis of rotation, it is also assumed that only one reaction wheel is on the spacecraft.

3. The spacecraft always knows its current angular position and angular velocity with perfect accuracy.

4. Solar radiation torque is constant and is calculated for the *worst case scenario* where the Sun is directly behind the spacecraft, and half of the surface facing the Sun reflects its light perfectly and the other half is shaded.

5. All attitude changes are small such that the torque from SRP remains constant.

6. The spacecraft is a cube with constant density.

7. For every time step of the simulation the reaction wheel can either be torqued upon or not. Each torque put on the reaction wheel has the exact same magnitude but may alternate direction.

8. The reaction wheel is operated in "minimum torque mode" where only enough torque is placed on it to change its RPMs by the minimum amount possible.

The model begins in the same way as attitude control model in Section 2.2.5 where the user specifies the mass and size of the cubeSat. The user then specifies the properties of the reaction wheel including: moment of inertia, J_{rw}, the minimum amount which the reaction wheels angular momentum can be changed, $\Delta\omega_{rw}$ in revolutions per minute (RPM) (later converted to radians per second), and the *reaction time*, t which is the time it takes the motor of the reaction wheel to change its speed by $\Delta\omega_{rw}$ in seconds. If the moment of inertia is not specified by the manufacturer then it may be approximated by the formula

$$J_{rw} = mR^2 \tag{2.33}$$

where m is the mass of the wheel in kilograms, and R is the radius of the wheel. This formula assumes that all of the mass of the reaction wheel is concentrated along the rim of the wheel.[34, 35] Next the minimum amount which the cubeSat angular velocity can be changed is calculated using

$$\Delta\omega_{sat} = \frac{J_{rw}\Delta\omega_{rw}}{J_{sat}} \tag{2.34}$$

where J_{sat} is the moment of inertia of the cubeSat given previously by Eq 2.25.[34, 35, 40] Thus from basic kinematics the angular acceleration on the satellite is given by

$$\alpha_{sat} = \frac{\Delta\omega_{sat}}{t} \tag{2.35}$$

The torque on the sat from the reaction wheel is

$$\tau_{sat} = J_{sat}\alpha_{sat} \tag{2.36}$$

The torque and acceleration from SRP is exactly the same as was calculated in Eqs 2.15 and 2.28.

The simulation runs the same as was described in Section 2.2.5 with each time step lasting for the *reaction time* t. When the algorithm decides whether to apply a positive or negative torque on the spacecraft the current position and velocity are updated using Eqs 2.30 and 2.31 while the speed of the reaction wheel is updated using

$$\omega_{rwnew} = \omega_{rwold} \pm \Delta\omega_{rw} \tag{2.37}$$

A sample output of the simulation is provided in Figure 2.4. This simulation corresponded to a 1U 2 kg cubeSat with a 50 g, 20 mm radius reaction wheel. The reaction time of the wheel was 0.1 s and the satellite successfully maintained a switching interval of 0.02 degrees.

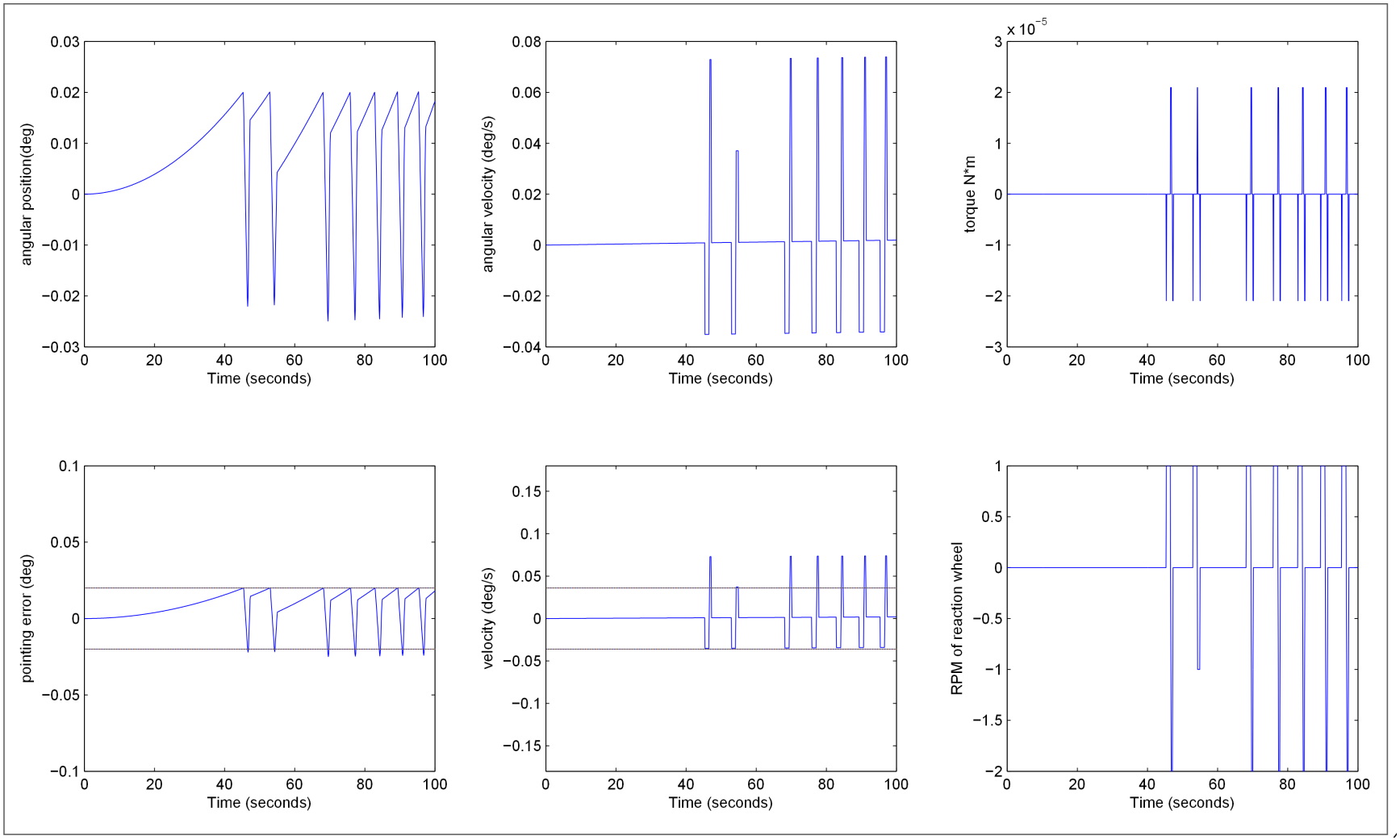

Figure 2.4: Sample output of attitude control simulation using reaction wheels.

2.3. COMPARISON OF CURRENT CUBESAT REACTION CONTROL SYSTEMS WITH PLASMONIC FORCE PROPULSION (PFP) THRUSTERS

Several new and developing micro propulsion systems for small satellites were studied and modeled using the algorithms presented in Section 2.2. This section documents the characteristics of each thruster system and compares its performance to that of PFP thrusters. The results of the simulations and a comparison of the characteristics of each thruster is summarized in Section 2.3.7.

2.3.1. Plasmonic Force Propulsion (PFP) Thrusters. Plasmonic Force Propulsion (PFP) thrusters are a novel new small sat RCS which function by using the light from the Sun to accelerate nanoparticles at high speed. The plasmonic force being used by the thruster to accelerate nanoparticles is similar to the optical force produced by the "optical tweezers" which biologists use to move viruses around.[11, 12]. Optical tweezers work by using the electric field gradient produced by a focused laser to move dielectric nanoparticles to the waist of the beam where the electric field is the strongest. PFP thrusters also use electric field gradients produced by light to accelerate nanoparticles, but are different from optical tweezers in that the electric field gradient is not produced by the concentrated light itself but rather by the interaction of the light with a nanostructure. It has been shown that plasmonic forces created by the interaction of light with metallic nanostructures can trap nanoparticles,[13, 14], but accelerating nanoparticles to create thrust has not yet been widely researched. Also, it should be noted, since there has previously been much confusion about this, that the interaction between light and the nanostructures produces a *potential ramp* not a *potential well*. A sample force and potential profile of a nanostructure is shown in Figure 2.5. The force and potential profiles seen in Figure 2.5 are for a nanostructure designed to resonate with 800 nm light. Observe that the plasmonic force is positive all the way through the structure reaching a maximum as the particle exits the structure. As the particle continues moving in the $+\hat{y}$ direction outside the structure the

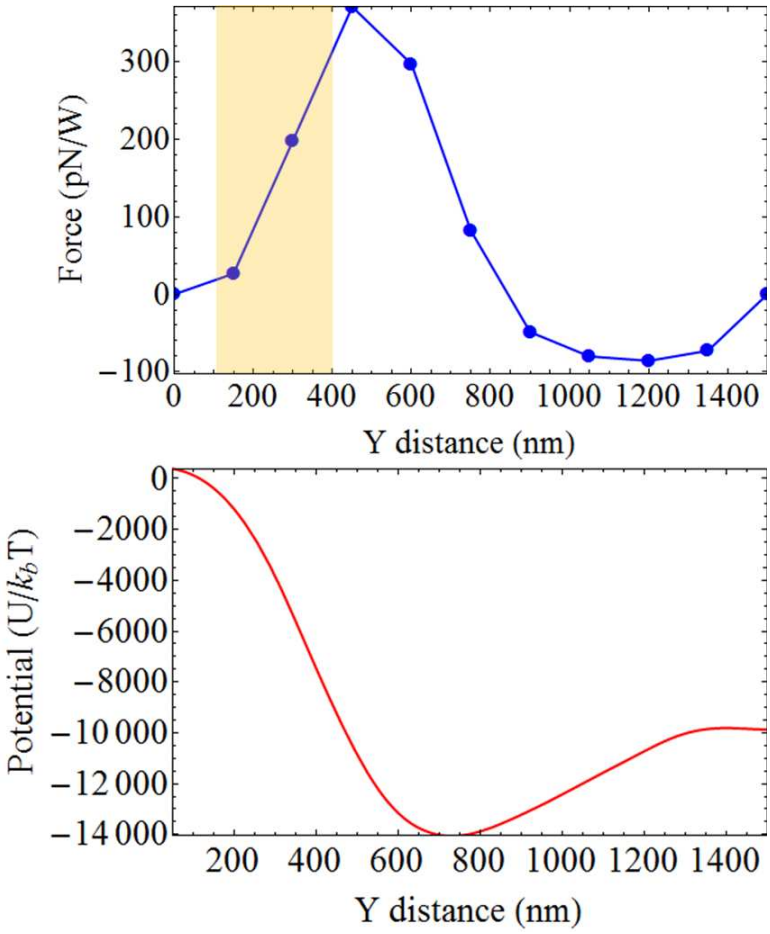

Figure 2.5: Force and potential profiles for a nanostructure designed to resonate with 800 nm light.
The nanostructure is 300 nm long and it is located from 100-400 nm (shown in gold)

force very quickly drops to zero then becomes slightly negative before returning to zero. However, this slight negative force, while it hinders the particles escape, is not enough to stop it completely. Thus it is possible for nanoparticles to be accelerated away from the structures without returning producing a net thrust.

PFP thrusters will work by focusing light from the Sun on an asymmetric nanostructure seen in Figure 2.6a. The light will resonate more strongly with the larger end of the metallic nanostructure than the smaller end. This discrepancy in light resonance will create an electric field gradient which is strongest at the large end of the structure seen

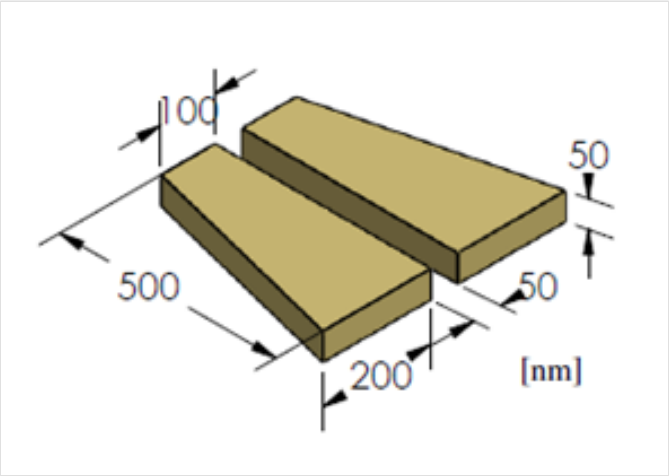

(a) A single stage of the nanostructure designed to resonate at 800 nm

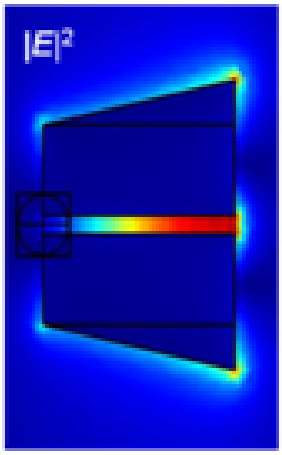

(b) The electric field distribution

Figure 2.6: Plasmonic nanostructure diagram and electric field.

in Figure 2.6b. The resulting gradient will cause neutral dielectric nanoparticles to be accelerated out the structure. By arranging several multi-stage layers of nanostructures with different resonant wavelengths as demonstrated in Figure 2.7 the nanoparticles should be accelerated to an appreciable speed. The exit velocity of the particles leaving a staged PFP thruster shown in Figure 2.7 can be increased by adding more resonant nanostructures above or below the nanotubes, by increasing the intensity of the incident light, or by increasing the length of the entire structure. Ultimately, a longer structure yields a greater exit velocity but the number of resonant nanostructures and the total length of the thruster will be limited by the method of manufacturing and assembling the nanostructures. Thrust can be increased by increasing the exit velocity or by adding more nanotubes and nanostructures for the particles to be accelerated through.

The size, configuration, and propellant type of PFP thrusters will be easily customizable to fit the needs of various missions. In this study a single thruster configuration consisting of an array of 3010, 5 mm long nanotubes each tube expelling 1×10^6 100 nm diameter polystyrene nanoparticles per second was used to obtain baseline thrust and spe-

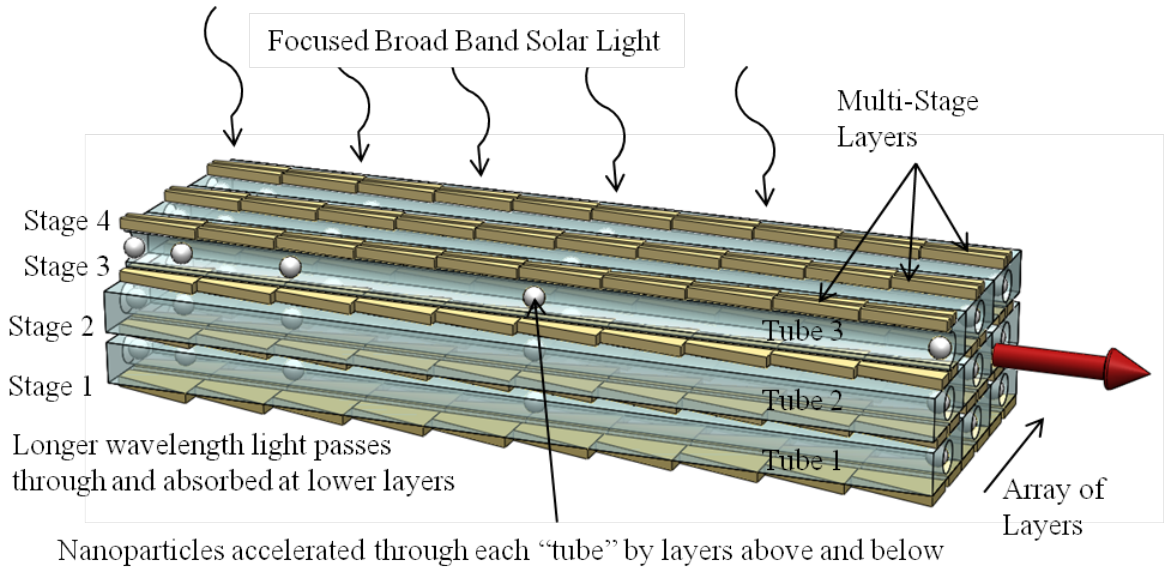

Figure 2.7: Diagram of the multi stage array of nanostructures interacting with light to accelerate nanoparticles.

cific impulse estimates. This baseline thruster is 35 nanotubes thick and 86 wide, on the top and bottom of each nanotube is a plasmonic nanostructure each designed to resonate with a different wavelength of light ranging from 1100 nm to 400 nm. Such a thruster would have a width of 52 μm and a thickness of 5 μm. By comparison a human hair is 70 μm in diameter. The mass of each thruster would be negligible so the system mass would be determined by the 5 cm diameter lens used to focus the light on the nanostructures and the total mass of the propellant used. It is estimated that such a multistage array plasmonic thruster with all the light from a 5 cm diameter lens focused on it would have a thrust of 107.5 nN and a specific impulse of 6.686 s.

As mentioned previously thrust and specific impulse can be customized by changing the thruster length, intensity of light, mass flow rate, the type of nanoparticle, and the size of the nanoparticles. Figures 2.8 and 2.9 shows how thrust and specific impulse change as the size and type of nanoparticles traveling through the tubes is changed. Greater thrusts and specific impulses than those shown in Figures 2.8 and 2.9 can be achieved by increasing

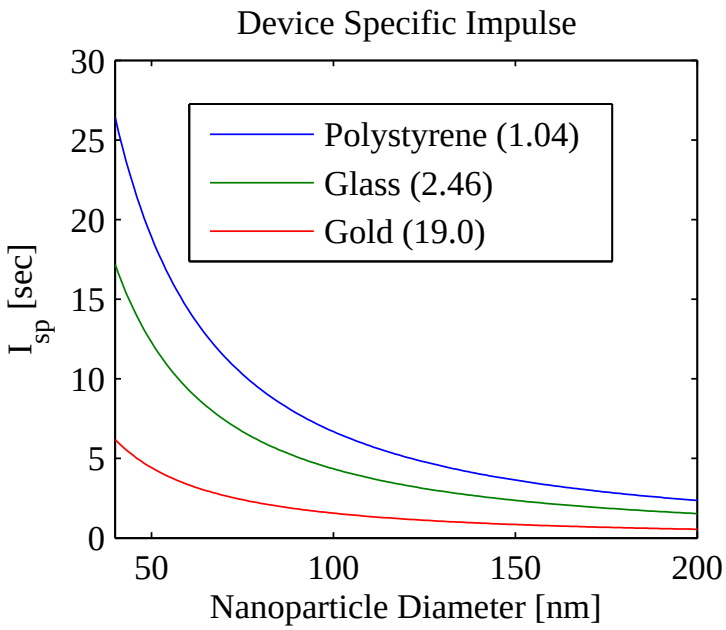

Figure 2.8: Specific impulse vs nanoparticle diameter for 5 mm long thrusters and 5 cm lens.

The densities in g/cm^3 are shown in parentheses.

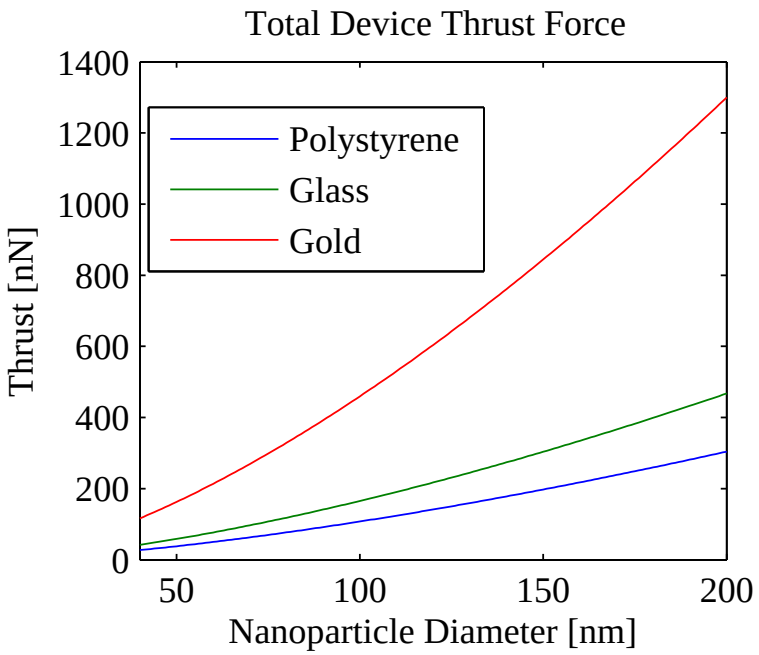

Figure 2.9: Thrust vs nanoparticle diameter for 5 mm long thrusters and 5 cm lens.

the light incident on the nanostructures by increasing the size of the collecting lens. There is a linear relationship between lens diameter, and thrust and specific impulse shown in Figures 2.10 and 2.11. Increasing the length of the nanotubes does not increase the thrust or specific impulse. The longer acceleration length does increase the thrust and the specific impulse, but the decreased light intensity due to increasing the total area which must be illuminated exactly cancels this. In summary PFP thrust can be increased by increasing lens or nanoparticle diameter. Specific impulse can be increased by increasing lens diameter and decreasing nanoparticle diameter. Specific impulse can also be improved by using lighter particles such as polystyrene. In this initial study three separate nanoparticle propellants were considered, gold, glass, and polystyrene; each having densities of 19.0, 2.46, and 1.04 g/cm^3 respectively. However, any number of nanoparticle propellants could be used depending on the missions required propellant density. As seen in Figures 2.8 and 2.9 denser propellants produce greater thrusts and lower specific impulses, while less dense propellants produce low thrusts but high specific impulses.

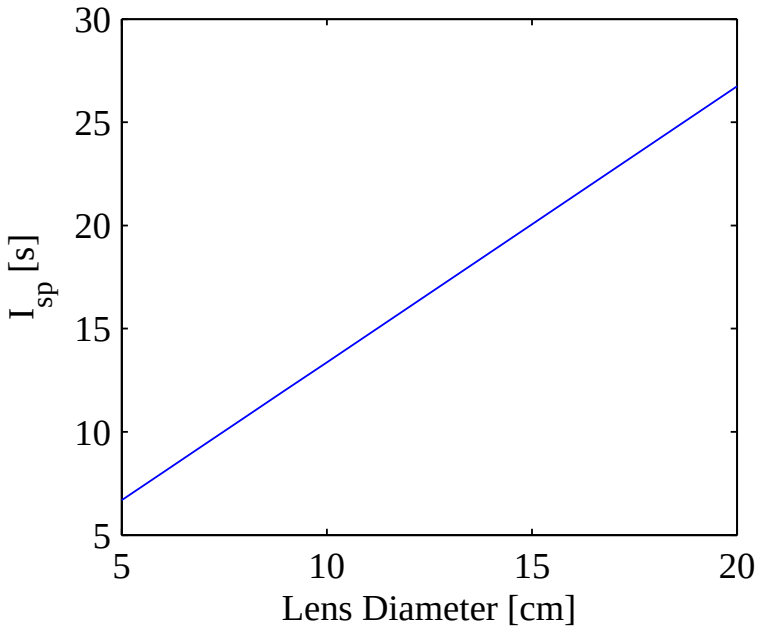

Figure 2.10: Specific impulse vs lens diameter for 100 nm polystyrene nanoparticles.

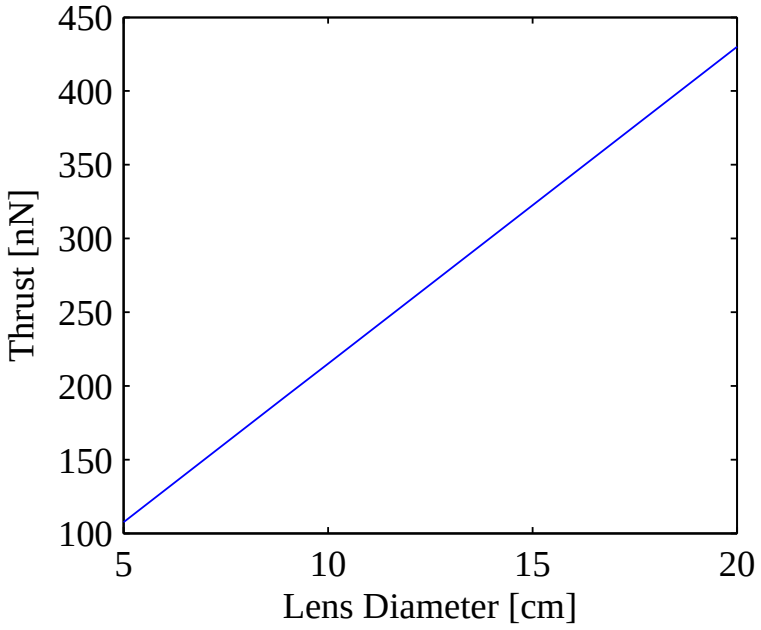

Figure 2.11: Thrust vs lens diameter for 100 nm polystyrene nanoparticles.

The switching time of PFP thrusters is currently not known and will be determined by how the thruster is actuated. Actuation of the thruster could be controlled by a mechanical shutter or electric glass allowing light to shine on the nanostructures, or an electronically controlled valve on the nanoparticle propellant tank or a combination of these. A mechanical shutter would allow for very fast switching times, high end cameras typically have shutter speeds higher than 1/10,000 of a second. However, the vibrations from a shutter could induce unwanted motion in the spacecraft. Electric glass using "micro-blinds" can change from opaque to transparent and back on the order of a millisecond but is still under development.[43]

One of the largest disadvantages to using PFP thrusters is their low specific impulse ranging from 1-25 s as seen in Figures 2.8 and 2.10. Other small satellite electric propulsion systems, such as μCAT, VAT, PPT, and Electrospray have much higher specific impulses ranging from 600-5000 s. However, PFP thrusters take up considerably less mass and volume than other thruster systems. The actual 5 mm long 52 μm wide thruster seen in

Figure 2.7, would have negligible mass and volume compared to the cubeSat. The entire mass of the system would be determined by the ~5 cm diameter lens and the mass of the nanoparticle propellants. It is estimated that the dry mass of the entire system could be as low as 50 g and occupy a volume of 50 cm^3. Assuming that the tanks are filled with another 100 g of propellant a 2 kg satellite with the $I_{sp} = 6.686$ s thrusters would have 3.4 m/s of ΔV. If a more efficient $I_{sp} = 11$ s thruster configuration was used the cubeSat could have 5.5 m/s of ΔV. Nanoparticle propellant tanks could be added or subtracted depending on a missions ΔV requirements. PFP thrusters would be well suited for cubeSat missions which require high accuracy pointing and position control where mass, power, and volume budgets are tight.

2.3.2. Micro-Cathode Arc Thrusters (μCAT). The Micro-Cathode Arc Thruster (μCAT) is currently under development at The George Washington University and is at TRL-4. The μCAT consists of a titanium cathode and a copper anode separated by an insulator. The copper anode is surrounded by an inductor which releases a high voltage pulse causing a discharge between the electrodes. The titanium cathode acts as the propellant and ablates during the discharge as a portion its surface is converted to plasma. The plasma is then accelerated out of the thruster being directed by the magnetic field of the inductor.[44–46]

The main advantages of the μCAT is that it has high I_{sp} (2000-3500 s), relatively high thrust (100 μN), and low mass (100 g per thruster)[45, 46]. A cubeSat using μCAT thrusters would also require a inductive pulsed power unit adding a mass of approximately 100 g. The titanium cathode acting as propellant has a mass of 40 g and density of 4.5 g/cm^3. Assuming that the entire Titanium cathode is consumed as propellant a 2 kg cubeSat equipped with a μCAT would have 400-700 m/s of ΔV meaning that the cubeSat would be able to easily perform orbital maneuvers besides station keeping. However, the μCAT is currently only estimated to have a lifetime of ~10^8 pulses, meaning with an impulse bit of 2 μNs, it will only be able to provide ~100 m/s of ΔV to a 2 kg cubeSat.[47]

With a switching time of 20 ms the μCAT can provide good pointing and positioning accuracy of 1×10^{-4} deg and 6×10^{-4} m. As a result of the relatively high thrust produced by the μCAT and larger switching time it is not as well suited for missions which require high accuracy pointing and proximity control as PFP thrusters.

2.3.3. Vacuum Arc Thrusters (VAT). The Vacuum Arc Thruster (VAT) developed by Alameda Applied Sciences Corporation uses a solid metal cathode as the propellant and is considered to be at TRL-5. A vacuum arc is an electric discharge which occurs in a vacuum between a heated cathode and an anode containing the solid metal propellant. A large number of metals are available as propellants including Titanium, Yttrium, Silver, Tantalum, and Tungsten, but the two most common are Titanium and Tungsten having densities of 4.5 g/cm^3 and 19.25 g/cm^3 respectively. Typically VATs use a 40 g Titanium anode as the propellant. As the electron beam strikes the propellant anode its surface becomes a plasma which is then accelerated away from the thruster at high speed.[48–51]. The VAT has an extremely large throttleable average thrust range of 10 nN to 300 μN a high specific impulse of 1000-3000 s and a fast switching time of 1 ms. The average thrust ranges from 10 nN to 300 μN, but this is done by altering the switching time of the thruster. The range of impulse bits is 10 nNs to 30μNs. Thus the lowest instantaneous thrust assuming a 1 ms switching time is 10 μN.[48]

With the combination of a wide range of throttleable thrusts and a fast switching time of 1 ms the VAT can maintain extremely low switching intervals. If used on a 2 kg cubeSat it could provide precision pointing to 2×10^{-7} degrees and position accuracy up to 4×10^{-11} m. With its high specific impulse it could provide 200-600 m/s of ΔV assuming it consumed the entire Titanium anode as propellant. However, the rated lifetime of the VAT is only 5 million pulses so each VAT is only able to provide ~75 m/s of ΔV to a 2 kg cubeSat. In addition to this the VATs 300 g PPU requires 10 W of power to operate,

The main advantages of the VAT are its large throttleable thrust range, low minimum impulse bit, and fast switching time which allow for extremely low switching intervals

at the limit of what a cubeSat can sense. However, its relatively short lifetime, high power consumption, and relatively large mass limit its utility on cubeSats.

2.3.4. Pulsed Plasma Thruster (PPT). PPTs were originally developed in the late 60s and were the first successful electric propulsion system used in space. They are easily scalable and have been used on a number of large satellites as both an ACS and RCS. PPTs commonly use solid PTFE (Teflon) as a propellant. The Teflon is ablated and converted to plasma through a high voltage electric discharge between two capacitor plates. the plasma is then accelerated away via the Lorentz force[52]

Clyde Space makes a small electric propulsion system for small satellites called the Pulsed Plasma Thruster (PPT) produces a thrust of 4.5 μN, has a switching time of 0.2 s and a specific impulse of 608 s. The thruster with all supporting systems comes in a $90 \times 90 \times 27$ mm envelope which conveniently fits into the back fourth of a 1U cubeSat.[53] It carries 7 g of Teflon propellant the density of which is 2.2 g/cm^3 which provides 21 m/s of ΔV for a 2 kg cubeSat. The thruster has a lifetime of 1.5 million pulses and is estimated to provide 42 Ns of total impulse. Currently there is no PPT designed to be used as an ACS on cubeSats and is primarily suited for extending the mission life of cubeSats by providing a small amount of ΔV to combat atmospheric drag. The main advantage of PPTs is that they are a flight proven technology, but they are not as small and efficient as newer thruster systems.

2.3.5. Electrospray Thrusters. Electrospray thrusters operate by accelerating electrically charged droplets of ionic liquids at high speeds using high voltage electric fields. Various Electrospray thruster designs vary widely and are constantly being improved. They have previously been used on larger satellites but MIT is currently developing a miniaturized version for use on cubeSats. Electrospray thrusters have a number of advantages such as high thrust (100 μN), high specific impulse (2500-5000 s), and have a short switching time (1 ms). Each thruster is very small, about the size of a penny, and is only a few grams. an exact mass estimate is not available since the thruster is still under development but

each one should have a mass under 10 g. Their main disadvantages are that they require a large high voltage power processing unit which draws 10 W of power, occupies a volume of ~300 cm^3 and adds 250-300 g to the system mass. MITs miniature Electrospray thrusters are expected to have an extremely long life and should give cubeSats relatively large amounts of ΔV. They will also provide both positioning and attitude control but not to the level of precision of PFP thrusters.[54–57]

2.3.6. Reaction Wheels. Currently there are not many cubeSat reaction wheels available but a new model which came out in the past year is the Blue Canyon Technologies Micro Reaction Wheel. It has a moment of inertia of 28.6×10^{-6} kg·m^2, mass of 150 g, volume of 33 cm^3, and a max torque of 0.6 mN·m. It only requires a maximum of 1 W of power and operates from 5-15 V. The wheel can reach a maximum speed of 6,000 RPM, and is expected to have a lifetime of 3 years.[58] For the purposes of the simulation it was assumed that the reaction wheel had a reaction time of 0.1 s. This gave a pointing accuracy of 0.01 degrees when placed on a cubeSat. Because of the large torques reaction wheels are able to provide they can turn a cubeSat much quicker than micropropulsion thrusters, however, they do not provide as fine of pointing accuracies.

2.3.7. Micropropulsion summary. Table 2.1 compares the characteristics of all the micropropulsion systems and reaction wheels considered in this thesis. As many of these thrusters are still in development and/or easily customizable the values presented in this table vary from source to source. Please see Sections 2.3.1 to 2.3.6 for more details.

Thruster type	PFP	μCAT	VAT	PPT	Electrospray	Reaction Wheels
Thrust used in Simulations	250 nN	100 μN	10 μN	4.5 μN	100 μN	N/A
Specific Impulse (s)	1-12	2000-3500	1000-3000	608	2500-5000	N/A
Switching Time (ms)	1	20	1	200	1	100
Pointing Accuracy (deg)	2×10^{-9}	1×10^{-4}	2×10^{-7}	N/A	1×10^{-6}	0.01
Position Accuracy (m)	3×10^{-12}	6×10^{-8}	4×10^{-11}	8×10^{-7}	6×10^{-10}	N/A
Min Impulse Bit (nNs)	50 pNs	2 μNs	10 nNs	900 nNs	100 nNs	N/A
Thruster Mass (g)	<0.001	100	90	280	<10	N/A
Supporting Systems Mass (g)	100	100	300	0	250	150
System Volume (cm^3)	50	200	200	220	300	33
Propellant Mass (g)	50-100	40	40	7	20	N/A
Propellant type	Nanoparticles	Metal (Ti)	Metal (Ti or W)	Teflon	Ionic Liquids	N/A
Propellant Density (g/cm^3)	1.04	4.5	4.5	2.2	varies	N/A
Max Power Required (W)	0	5	10	2.7	10	1
ΔV for 2kg cubeSat (m/s)	1-6	~100	~75	21	250-500	N/A
Lifetime (pulses)	unknown	10^8	5×10^6	1.5×10^6	unknown	three years
Configurable as ACS?	yes	yes	yes	no	yes	yes
Scalable/Customizable?	yes	yes	yes	no	yes	yes
Throttleable?	yes	no	yes	no	yes	yes
High Voltage Required?	no	yes	yes	yes	yes	no

Table 2.1: Comparison of various cubeSat propulsion systems.

2.4. CHALLENGES ASSOCIATED WITH THE DEVELOPMENT AND USE OF PFP THRUSTERS AND POSSIBLE SOLUTIONS

This section will address some of the practical issues with using PFP thrusters from a mission standpoint and offer solutions.

2.4.1. How Does Light Get to Shaded Thrusters?. One of the most obvious issues with PFP thrusters is how to power thrusters which are in the shadow of the satellite itself. This could be solved by adding a Solar Light Allocation Pipe or SLAP to the PFP thruster system. The SLAP would be a system of fiber optics to pipe light to the needed thrusters something like the design shown in Figure 2.12. This however would add mass and volume to the system.

A SLAP is necessary for precision attitude control and proximity control. In order to perform attitude control maneuvers without changing the satellites orbit, thrusters on both sides of the satellite must be fired simultaneously to null translational motion. This

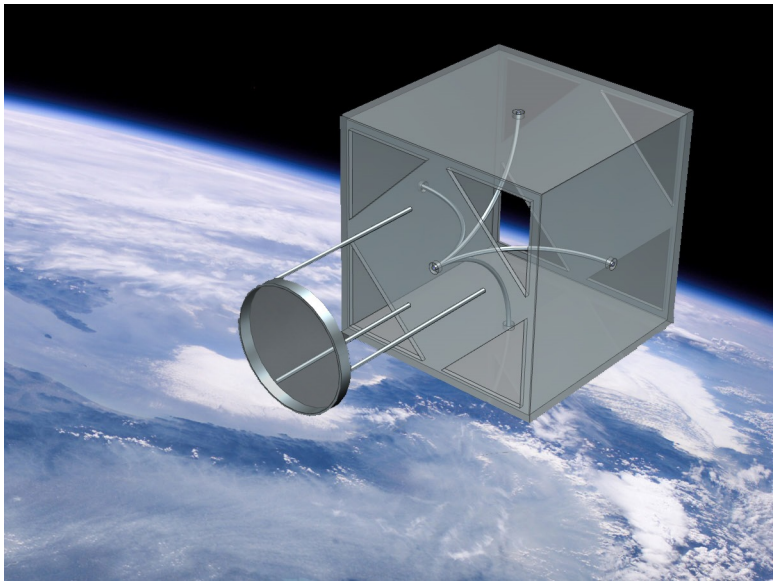

Figure 2.12: CubeSat over earth using PFP thrusters powered by the SLAP (Solar Light Allocation Pipe).
Thrusters are not shown but are parallel to the faces of the cubeSat where the fiber optic cables terminate.

was an integral assumption of the attitude control model. The SLAP is also necessary for proximity control. In order to change position with respect to another satellite a cubeSat must perform two maneuvers to start and stop its motion. Each maneuver will require thrusters on opposite sides of the cubeSat to fire, meaning one of the thrusters will be shaded and unable to fire.

Furthermore, getting the lens to focus the light on the plasmonic thrusters or into the SLAP could prove difficult. In order for Sun light to be focused on a point by a lens the lens must be perpendicular to the incoming rays and the distance between the lens and the point must be equal to the focal length of the lens.[28] As the attitude of the cubeSat changes the lens or the thrusters must move in order to remain in focus. However, adding moving parts will add more mass, volume, complexity, and cost to the system. Furthermore, moving parts will produce a torque on the spacecraft which will decrease pointing accuracy and use up a significant amount of propellant. This would not be an issue on a larger spacecraft employing two separate attitude control systems. If the spacecraft needed to change its attitude, before making the maneuver it could move/rotate the lens such that it would be lined up with the future location of the SLAP. Then the spacecraft could make the maneuver using its primary coarse ACS then use PFP thrusters for fine control.

2.4.2. What Happens When in the Shadow of the Earth?. Since PFP thrusters are powered by Sunlight they cannot be operated when in the shadow of the earth or otherwise not illuminated. This is a problem which can only be avoided by placing the spacecraft in an orbit which does not cross into the earths shadow. However, it should be noted that when the spacecraft is in shadow the primary disturbance force, solar radiation pressure, will not be disturbing the spacecraft. Thus, attitude control will not be as critical when operating in the shadow of the earth.

2.4.3. Improving Thrust and Specific Impulse. Finally the biggest challenges to PFP thrusters is their low specific impulse. The estimated 1-6 m/s of ΔV is is only useful for short periods of time formation flying with other satellites or for attitude control. As

a result PFP thrusters will not be able to be used to change a spacecrafts orbit or extend the life of cubeSat missions significantly. The best ways to increase specific impulse are to increase the intensity of light striking the nanostructures or to increase the efficiency at which the nanostructures convert light into thrust. Adding a larger lens adds more mass and the small size of cubeSats limits the diameter of any collection lens at 10 cm. Clearly it is more advantageous to have more efficient structures, however, it is currently not known whether or not more efficient structures can be produced.

The intensity of the light upon the structures can be increased by keeping the lens size constant but decreasing the size of the structure. As mentioned previously increasing or decreasing the thruster length has no effect on the thrust and specific impulse because the effect of increasing the acceleration length exactly cancels the effect of decreasing intensity due to increasing incident area. However, decreasing thruster width increases the intensity and thus the force on each individual nanostructure while leaving the acceleration length the same. This deceases the number of nanotubes expelling particles and thus the thrust but increases the speed at which the particles exit the tubes increasing specific impulse. A PFP thruster 35 nanotubes wide and 35 thick would have a specific impulse of 10.48 s and thrust of 68.5 nN. A non realistic but limiting PFP thruster design which had a single layer of 35 nanotubes and all the light from a 5 cm diameter lens focused on it would have a specific impulse of 62 s and thrust of 11.6 nN.

2.4.4. Manufacturing PFP Thrusters. It is currently very difficult to manufacture nanostructures on a macroscopic level. Even making arrays of nanostructures 5 mm long is difficult using current techniques. However, researchers at the Missouri University of Science and Technology are currently working on a new method of manufacturing nanostructures known as *Nanosphere Photolithography*.[59–61] It is hypothesized that this technique could allow nanostructures covering an area as large as 1 m^2 to be produced. If this technique proves to be effective then it would be possible to create PFP thrusters along the entire length of a cubeSat.

2.5. CONCLUSIONS

PFP thrusters are a promising new propulsion system for both cubeSats and other small satellites which can be used as both an RCS and ACS. While they do not provide as much ΔV as other cubeSat propulsion systems they require no power, and are extremely low mass and volume. Their low thrust and short switching time makes them ideal for missions where exact distances between spacecraft must be maintained or missions which require extremely high pointing capabilities. A cubeSat employing PFP thrusters would be able to maintain at attitude which was only limited by its attitude sensing instruments.

The ultra low thrust of PFP thrusters could also be used for attitude or proximity control on larger satellites. NASAs Laser Interferometer Space Antenna mission to detect gravitational waves requires that the satellites know their positions relative to each other and maintain precise orbits to with respect to each other. The LISA spacecraft will not be formation flying and the distance between them will be constantly changing but needs to be constantly known to within 20 pm over 5,000,000 km. As a result, this mission will require extremely precise reaction control thrusters with thrusts on the order of a micro-newton or less.[15–17] PFP thrusters can position a cubeSat accurately to within 3 pm, meaning they could position a larger satellite with greater precision making them a viable option for the LISA mission or future NASA missions which require greater precision.

PFP thrusters are also a viable option for the NASA proposed Stellar Imager or SI mission. This mission concept consists of 20-30 formation flying "mirror sats" each one a meter diameter mirror precisely placed to within 5 nm over several kilometers. Each mirror sat will also have to control its attitude to less than 0.76 milliarcseconds. The entire Interferometer telescope will allow 0.1 milliarcsecond resolution images of stellar surfaces and the universe in general to be taken.[18–20] It is estimated that PFP thrusters can provide pointing accuracy to within 2×10^{-9} degrees or 0.0072 milliarcseconds or 7.2 microarcseconds for a cubeSat. Each mirror sat will be a 1 m diameter mirror segment only a few times

larger than a cubeSat so it is reasonable to expect a "mirror sat" employing PFP thrusters to have pointing accuracies comparable to those predicted for a cubeSat.

Future Work. While many challenges face the development of PFP thrusters more research is needed to experimentally determine and improve their performance. Future research should primarily focus on:

1. Experimentally verifying that the forces produced by a single nanostructure on a single nanoparticle match those predicted for a given incident light intensity.

2. Both by simulation and experimentation determining ways of increasing the specific impulse of PFP thrusters.

3. Improving the efficiency at which the nanostructures convert incident light energy into kinetic energy of the particle either by improving the designs of current nanostructures or by developing new designs or using new materials.

4. Developing the SLAP by having a detailed working model of exactly how light will be delivered to each thruster and what intensity it will be.

5. Researching in detail various actuation mechanisms for PFP thrusters such as mechanical shutters and electric glass.

6. Experimentally verifying that the forces produced by an array of nanostructures produce thrusts and specific impulses predicted.

7. Developing a method of delivering nanoparticles from the propellant tanks to the thruster nanotubes.

8. Determining which nanomanufacturing techniques are best for producing and assembling the large arrays of nanostructures used in PFP thrusters.

Items 1-3 are of primary concern and should be the main research goals of phase II of the NIAC study, while items 4, and 5 should be secondary objectives. Items 6-8 are the most important to the use of PFP thrusters, but are beyond the scope of the phase II NIAC study.

3. CONCLUSIONS

The first half of this thesis low pressure performance of SDBD plasma actuators was investigated at pressures ranging from 10-101 kPa. The effects of buried and exposed electrode length, as well as chord-wise gap, on actuator thrust production and effectiveness were studied. It was found that increasing the buried electrode length improved thrust the most, while increasing the gap length decreased thrust but increased effectiveness. Altering exposed electrode length had little to no effect on thrust or effectiveness.

The actuator which produced the most thrust overall had a buried electrode length of $b = 75$ mm. This design produced 26% more thrust at all pressures than the baseline $b = 15$ mm design and produced 34% more thrust between the pressures of $20 - 40$ kPa. As buried electrode length is increased, the electric field extends farther downstream, thus as buried electrode length increases, thrust production increases, particularly at low pressure where more plasma is created. Because they produce the most thrust plasma actuators with long chord-wise buried electrode lengths will offer more aerodynamic control to aircraft in low pressure environments.

The second half of this thesis focused on PFP thrusters, which are a promising new space propulsion system for both cubeSats and larger spacecraft requiring extremely high pointing accuracy. PFP thrusters consist of an array of sub-wavelength metal nanostructures which resonate when interacting with light. The interaction between the light and the nanostructures produces an electric field gradient within the structure which can be used to accelerate nanoparticles at high speeds.

PFP thrusters are expected to have a thrust of 50-500 nN and a switching time of 1 ms. Their low thrust and high switching time gives them the ability to position spacecraft with great accuracy. It is expected that PFP thrusters will give cubeSats the ability to fly in formation with 3 picometer precision and have pointing accuracies on the order of

0.01 milliarcseconds. In addition to this PFP thrusters are extremely low mass and are approximately the size of a human hair. It is estimated that 16 PFP thrusters providing six degrees of freedom and all the supporting systems such as the collecting lens would only have a mass of 100 g and occupy a volume of 50 cm^3. The small size and expected high precision capabilities of PFP thrusters make them a potential enabling technology for future NASA missions such as the Laser Interferometer Space Antenna and The Stellar Imager.

PFP thrusters have been shown to be a promising technology but they face several challenges. Future research on PFP thrusters should focus on experimentally verifying that the nanostructures interact with light in the way predicted, improving the specific impulse of PFP thrusters, and developing methods of actuating PFP thrusters.

APPENDIX A

MATLAB PROXIMITY CONTROL MODEL USING RCS THRUSTERS

```
\begin{code}

%function [] = BangBangXv2()
%
%Filename:BangBangXv2.m
%Author: Paul D. Friz
%Contact: pdfriz@gmail.com
%Advisor: Joshua L. Rovey (roveyj@mst.edu)
%Affiliation: Missouri University of Science and Technology, Aerospace
%Plasma Lab, Aerospace Enigneering Dept
%Purpose: Models the proxcimity control capabilities of cubeSats using
%reaction control thrusters such as Electrospray, Plasmonic Interaction
%MicroPropulsion, Vacume Arc Thrusters etc.
%Detailed Description:
%Models a single axis Bang Bang or on/off controller for small satellites
%using reaction control thrusters. This version models proxcimity control
%of one space craft to another in the presence of solar radiation pressure.
%The assumptions of this model are:
%1.  There are no outside forces affecting the motion of the spacecraft
%other than its thrusters and solar radiation pressure.
%2.  The spacecraft always knows its current position and velocity with
%perfect accuracy.
%3.  The point/object/other satellite which the spacecraft is trying to
%maintain proximity to is inertially fixed.
%4.  Solar Radiation Pressure acts only along the x-axis. Also the solar
%radiation pressure is constant and is calculated for the "worst case
%scenario" where the sun is directly behind the spacecraft and the
%spacecrafts surfaces reflect light perfectly back toward the sun.
%5.  Spacecraft is a cube with constant density
%6.  For every time step of the simulation the thrusters can either be
%fired or not fired. There is no "recharge time" for the thrusters and
%each burst delivers the same impulse for the same amount of time.
%7.  This is a single axis simulation so all forces (thrust and SRP) act
%only along that axis.
%8.  The attitude of the spacecraft remains constant such that one face is
%always directly facing the sun.
%Spacecraft inputs are spacecraft mass and size. Thruster inputs are
%thrust, specific impulse, and the switching time of the thruster. Control
%inputs are switching interval, innitial posion and velocity, as well as
%set position
%

%Spacecraft Inputs
M = 2; %Spacecraft mass (kg)
L = .1; %length of side of cube sat (m)
%spacecraft calculations
```

```
SA = L^2; %surface area of one side of the spacecraft (m^2)

%Thruster Inputs
Isp = 2.9; %specific impuls of thruster (s)
switchT = .001; %switching time of thruster (s)
Thrust = 250e-9; %Thrust of thruster (N)
n = 2; %number of thrusters firing for particular manuver
g = 9.8; %acceleration due to gravity used to calculate exit velocity (m/s
    ^2)
Mp = .050; %mass of propellant on spacecraft (kg)
%spacecraft calculations
F = Thrust*n; %combined thrust of all thrusters firing (N)
Vexit = g*Isp; %exit velocity of exaust leaving thruster. (m/s)
ImpulseBit = Thrust*switchT; %impulse from one burst from one of the
    thrusters (kg*m/s)
deltaV = Vexit*log(M/(M-Mp)); %total delta V possible with propellant (m/s)

%Control inputs
setX = 0; %set/desired X position (m)
initialX = 1e-10; %starting X position (m)
initialV= 0; %starting velocity in (m/s)
switchInt = 2e-12; %the switching interval (m)
%innitialize position and velocity
X = initialX; %current x position (m)
V = initialV; %current velocity (m/s)

%Calculated parameters
a = F/M; %acceleration of space craft from thrusters firing (m/s^2)
delX = .5*a*switchT^2; %the smallest change in position possible from firing
     the thruster (m)
delV = a*switchT; %the smallest change in velocity possible. (m/s)

%worst case senario solar radiation pressure force. Assuming sun is shining
%directly upon one face of the cube sat and that face is perfectly
%reflective
Fe = 1360; %solar flux constant at 1 AU (W/m^2)
c = 2.99792458e8; %speed of light (m/s)
P = Fe/c; %solar radiation pressure SRP (N/m^2)
Fs = 2*P*SA; %solar radiation force assuming all light is reflected 180deg (
    N)
aSolar = Fs/M; %acceleration due to solar radiation pressure (m/s^2)
disDelX = .5*aSolar*switchT^2; %distance the sat will move due to SRP during
     one iteration of simulation (m)
disDelV = aSolar*switchT; %chang in angular velocity from SRP during one
    iteration (m/s)
```

```
iterations = 200; %number of iterations for simulation
simTime = iterations*switchT; %length of the simulation (s)
XArray = zeros(1,iterations); %creating array to store postion data
VArray = zeros(1,iterations); %creating array to store velocity data
thrusterTimerArray = zeros(1,iterations); %creating an array to store
    thruster use times.
timeArray = zeros(1,iterations); %creating an array to store time values.
thrusterTimer = 0; %the amount of time the thruster has been firing. (s)
ThrustArray = zeros(1,iterations); %creating an array to store thrust values
    .
errorArray = zeros(1,iterations);

status = 1;
stop = 0; %if stop = 1 the sattellite will decellerate constantly untill it
    stops or reaches the switchInt
for t=1:iterations; %t is the simulation timer each iteration is a time step
     equal to the length of the switching time of the thruster
    errorX = X - setX; %the difference between the current attitude and the
        set attitude
    XStop = .5*V^2/a; %the minimum distance it will take the satelite to stop
         moving assuming constant decelleration
    if abs(errorX) > switchInt + .1*switchInt %check to see if the craft is
        within 10% of switchTheta
        status = 0; % if position > 10% out of switchTheta then thrusters are
             not keeping craft stable enough
    end
    if sign(errorX) == sign(V) %if spacecraft is moving away from desired
        position end stop command
        stop = 0;
    end
    if abs(errorX) <= switchInt %when inside the switching interval
        stop = 0; %if inside switch int end stop command
        if abs(V) >= delV && V > 0 && errorX > 0 %if velocity + and moving
            away kill speed
            Force = -F;
        elseif abs(V) >= delV && V < 0 && errorX < 0 %if velocity - and
            moving away kill speed
            Force = F;
        else
            Force = 0;
        end
    elseif errorX > switchInt %when "above" the switchInt
        if errorX < XStop && V < 0 && stop == 0 %give command to stop if
            moving fast enough to overshoot
            stop = 1;
            Force = F;
```

```
    elseif stop == 1 && errorX < XStop %slow motion in order to stop
        Force = F;
    elseif stop == 1 && errorX >= XStop %coasting toward desired position
         to avoid stopping short
        Force = 0;
    else %accelerate toward desired postion
        Force = -F;
    end
elseif errorX < -1*switchInt %when "below" the switching interval
    if errorX > -1*XStop && V > 0 && stop == 0 %give command to stop if
        moving fast enough to overshoot
        stop = 1;
        Force = -F;
    elseif stop == 1 && errorX > -1*XStop %slow motion in order to stop
        Force = -F;
    elseif stop == 1 && errorX <= -1*XStop %coasting toward desired
        position to avoid stopping short
        Force = 0;
    else %accelerate toward desired posistion
        Force = F;
    end
else %if non of the above conditions are met take no aciton/coast
    Force = 0;
end

if Force == F %firing thrusters in positive direction
    X = X + delX + disDelX + V*switchT; %effects of thrusters, SRP, and
        current velocity on position
    V = V + delV + disDelV; %effects of thrusters and SRP on velocity
    thrusterTimer = thrusterTimer + switchT; %log thruster time
elseif Force == -F %firing thrusters in negative direction
    X = X - delX + disDelX + V*switchT; %effects of thrusters, SRP, and
        current velocity on position
    V = V - delV + disDelV; %effects of thrusters and SRP on velocity
    thrusterTimer = thrusterTimer + switchT; %log thruster time
else %F == 0
    X = X + disDelX + V*switchT; %if thrusters not fired SRP and current
        velocity will change current position
    V = V + disDelV; %if thrusters no fired SRP will change current
        velocity
end

XArray(1,t) = X; %storing the current X
VArray(1,t) = V; %storing current V
thrusterTimerArray(1,t) = F*thrusterTimer/(Vexit)*10e6; %converting
    thruster operating time to mass of propellant used in mg
```

```
    timeArray(1,t) = t*switchT;
    ThrustArray(1,t) = Force;
    errorArray(1,t) = errorX;
end

display(status)

figure

subplot(3,2,1); %spacecraft position plot
plot(timeArray,XArray)
axis([0 simTime min(XArray) max(XArray)])
xlabel('Time (seconds)')
ylabel('x position(m)')

subplot(3,2,2); %spacecraft velocity plot
plot(timeArray,VArray)
xlabel('Time (seconds)')
ylabel('velocity (m/s)')

subplot(3,2,6); %plot of fuel used with respect to time
plot(timeArray,thrusterTimerArray)
xlabel('Time (seconds)')
ylabel('mass of propellant used (mg)')

subplot(3,2,5); %plot of thrust level with respect ot time
plot(timeArray,ThrustArray)
xlabel('Time (seconds)')
ylabel('Thrust (N)')
axis([0 simTime -2*F 2*F])

subplot(3,2,3) %plot of position error with respect to time
plot(timeArray,errorArray, timeArray, switchInt, '--', timeArray, -switchInt
    , '--')
axis([0 simTime -5*switchInt 5*switchInt])
xlabel('Time (seconds)')
ylabel('position error (m)')

subplot(3,2,4) %plot of position error with respect to time
plot(timeArray,VArray, timeArray, delV, '--', timeArray, -delV, '--')
axis([0 simTime -5*delV 5*delV])
xlabel('Time (seconds)')
ylabel('velocity (m/s)')


\end{code}
```

APPENDIX B

MATLAB ATTITUDE CONTROL MODEL USING RCS THRUSTERS

```
\begin{code}

function [] = BangBangv2()
%
%Filename:BangBangv2.m
%Author: Paul D. Friz
%Contact: pdfriz@gmail.com
%Advisor: Joshua L. Rovey (roveyj@mst.edu)
%Affiliation: Missouri University of Science and Technology, Aerospace
%Plasma Lab, Aerospace Enigneering Dept
%Purpose: Models the pointing capabilities of cubeSats using reaction
%control thrusters such as Electrospray, Plasmonic Interaction
%MicroPropulsion, Vacume Arc Thrusters etc.
%Detailed Description:
%Models a single axis Bang Bang or on/off controller for small satellites
%using reaction control thrusters. This version models attitude control
%of a cubeSat in the presence of solar radiation pressure with it's
%thrusters mounted in the center of each face.
%The assumptions of this model are:
%1.  There are no outside forces affecting the rotation of the spacecraft
%other than its thrusters and solar radiation pressure.
%2.  This is a single axis simulation so all torques (thrust and SRP) act
%only along that axis of rotation.
%3.  The spacecraft always knows its current angular position and angular
%velocity with perfect accuracy.
%4.  SRP causes a constant torque in only one direction and is calculated
%for the "worst case senario" where the sun is directly hitting one face of
%the cubeSat, that face is half shaded, and the illuminated half of the
%spacecraft is perfectly reflecting sun light back toward the sun.
%5.  All attitude changes are small such that the torque from SRP remains
%constant.
%6.  Spacecraft is a cube with constant density.
%7.  For every time step of the simulation the thrusters can either be
%fired or not fired. There is no "recharge time" for the thrusters and
%each burst delivers the same impulse for the same amount of time.
%8.  Since fuel consumed during the simulations is very small (usually less
%than 1mg) the spacecraft is assumed to have constant mass.
%Spacecraft inputs are spacecraft mass and size. Thruster inputs are
%thrust, specific impulse, number of thrusters, and the switching time of
%the thruster. Control inputs are switching interval, innitial posion and
%velocity, as well as set position.
%

%conversions
DegtoRad = pi/180; %degrees to radians
RadtoDeg = 180/pi; %radians to degrees
```

```
%Spacecraft parameters
M = 2 ; %Wet mass of cubesat in kg
L = .1; %length of side of cube sat in meters
%spacecraft clacluations
r = L/2; %moment arm of thruster in meters
SA = L^2; %surface area of one face of the sat

%Thruster Inputs
Isp = 2.9; %specific impulse of thruster (s)
switchT = .001; %switching time of thruster (s)
Thrust = 50e-9; %Thrust of thruster (N)
n = 2; %number of thrusters firing for particular manuver (should be even
    number)
g = 9.8; %acceleration due to gravity used to calculate exit velocity (m/s
    ^2)
Mp = .050; %mass of propellant on spacecraft (kg)
%spacecraft calculations
F = Thrust*n; %combined thrust of all thrusters firing (N)
Vexit = g*Isp; %exit velocity of exaust leaving thruster. (m/s)
ImpulseBit = Thrust*switchT; %impulse from one burst from one of the
    thrusters (kg*m/s)
deltaV = Vexit*log(M/(M-Mp)); %total delta V possible with propellant (m/s)

%Control inputs
setAtt = (0)*DegtoRad; %set/desired attitude (rad) (parenthetical input in
    deg)
initialAttitude = -5e-8; %starting attitude (deg)
initialAngularVelocity = 0; %starting angular velocity (deg/s)
switchTheta = (1e-9)*DegtoRad; %the switching interval (rad) (parenthetical
    input in deg)
%initilaze attitude and angular velocity and convert to rad
curAtt = initialAttitude*DegtoRad; %current attitude (rad)
omega = initialAngularVelocity*DegtoRad; %current angular velocity in (rad/s
    )


%Calculated parameters
Icube = (M*L^2)/6; %moment of inertia of cube sat (kg*m^2)
tRCS = r*F; %torque on space craft from thrusters (N*m)
aRCS = tRCS/Icube; %angular acceleration of cube sat from thruster firing (
    rad/s^2)
delTheta = .5*aRCS*switchT^2; %change in angle from firing thrusters for
    switching time (rad)
delOmega = aRCS*switchT; %change in angular velocity from firing thrusters
    for switching time (rad/s)
```

```
%twirl = tRCS*switchT;

iterations = 200;
simTime = iterations*switchT; %the time of the simulation in s
positionArray = zeros(1,iterations); %creating array to store postion data
velocityArray = zeros(1,iterations); %creating array to store velocity data
propellantUseArray = zeros(1,iterations); %creating an array to store
    thruster use times.
timeArray = zeros(1,iterations); %creating an array to store time values.
thrusterTimer = 0; %the amount of time the thruster has been firing.
torqueArray = zeros(1,iterations); %creating an array to store torque values
    .
errorArray = zeros(1,iterations);

%worst case senario solar radiation pressure torque. Assuming sun is sining
%directly upon one face of the cube sat, that face is perfectly
%reflective and half of it is shaded.
Fe = 1360; %solar flux constant (W/m^2)
c = 2.99792458e8; %speed of light (m/s)
P = Fe/c; %Solar Radiation Pressure SRP (N/m^2)
Fs = 2*P*SA/2; %solar radiation force assuming all light is reflected 180deg
     (N)
tSolar = Fs*L/4 %torque caused by half of a side of the sat being
    illuminated (N*m)
alphaSolar = tSolar/Icube; %acceleration due to solar radiation pressure (
    rad/s)
disDelTheta = .5*alphaSolar*switchT^2; %angle sat rotates due to SRP during
    raction time (rad)
disDelOmega = alphaSolar*switchT; %the change in angular velocity due to
    disturbance torques. (rad/s)


stop = 0; %innitilize stop command status
status = 1; %innitilize status
for t=1:iterations; %t is the simulation timer
    errorTheta = curAtt - setAtt; %the difference between the current
        attitude and the set attitude
    thetaStop = .5*omega^2/aRCS; %the minimum angular distance it will take
        the satellite to stop rotating at its current angular speed assuming
        constant decelleration
    if abs(errorTheta) > switchTheta + .1*switchTheta %check to see if the
        craft is within 10% of switchTheta
        status = 0; % if position > 10% out of switchTheta then thrusters are
             not keeping craft stable enough
    end
```

```
if sign(errorTheta) == sign(omega)
    stop = 0;
end

if abs(errorTheta) <= switchTheta
    stop = 0;
    if abs(omega) >= delOmega && omega > 0 && errorTheta > 0 %kill +
        velocity inside of switchInt
        torque = -tRCS;
    elseif abs(omega) >= delOmega && omega < 0 && errorTheta < 0 %kill -
        velocity inside of switchInt
        torque = tRCS;
    else
        torque = 0;
    end
elseif errorTheta > switchTheta %when "above" the switchInt
    if errorTheta < thetaStop && omega < 0 && stop == 0 %give signal to
        stop if moving fast enough to overshoot
        stop = 1;
        torque = tRCS;
    elseif stop == 1 && errorTheta < thetaStop %stoping
        torque = tRCS;
    elseif stop == 1 && errorTheta >= thetaStop %costing toward desired
        attitude to avoid stopping short
        torque = 0;
    else %accelerate toward desired theta
        torque = -tRCS;
    end
elseif errorTheta < -1*switchTheta %when "below" the switching interval
    if errorTheta > -1*thetaStop && omega > 0 && stop == 0 %give command
        to stop to prevent overshooting
        stop = 1;
        torque = -tRCS;
    elseif stop == 1 && errorTheta > -1*thetaStop %stopping
        torque = -tRCS;
    elseif stop == 1 && errorTheta <= -1*thetaStop %costing to avoid
        stopping short
        torque = 0;
    else %accelerate toward desired theata
        torque = tRCS;
    end
else
    torque = 0;
end

if torque == tRCS
```

```
        curAtt = curAtt + delTheta + disDelTheta + omega*switchT;
        omega = omega + delOmega + disDelOmega;
        thrusterTimer = thrusterTimer + switchT;
    elseif torque == -tRCS
        curAtt = curAtt - delTheta + disDelTheta + omega*switchT;
        omega = omega - delOmega + disDelOmega;
        thrusterTimer = thrusterTimer + switchT;
    else
        curAtt = curAtt + disDelTheta + omega*switchT; %effect of
            disturbances on position
        omega = omega + disDelOmega; %effect of disturbances on angular
            velocity
    end
    positionArray(1,t) = curAtt*RadtoDeg; %converted back to deg
    velocityArray(1,t) = omega*RadtoDeg; %converted back to deg/s
    propellantUseArray(1,t) = F*thrusterTimer/(Vexit)*10e6; %total propellant
         used (mg)
    timeArray(1,t) = t*switchT;
    torqueArray(1,t) = torque;
    errorArray(1,t) = errorTheta*180/pi;
end

display(status)
display(deltaV)
display(ImpulseBit)



figure
subplot(2,3,1); %spacecraft attitude plot
plot(timeArray,positionArray)
xlabel('Time (seconds)')
ylabel('angular position(deg)')

subplot(2,3,2); %spacecraft velocity plot
plot(timeArray,velocityArray)
xlabel('Time (seconds)')
ylabel('angular velocity (deg/s)')

subplot(2,3,6);
plot(timeArray,propellantUseArray)
xlabel('Time (seconds)')
ylabel('mass of propellant used (mg)')

subplot(2,3,3);
plot(timeArray,torqueArray)
```

```
xlabel('Time (seconds)')
ylabel('torque (N m)')
axis([0 simTime -2*tRCS 2*tRCS])

subplot(2,3,4)
plot(timeArray,errorArray, timeArray, switchTheta*180/pi, '--', timeArray, -
    switchTheta*180/pi, '--')%,timeArray, sign(torqueArray)*switchTheta*360/
    pi, 'red')
axis([0 simTime -5*switchTheta*180/pi 5*switchTheta*180/pi])
xlabel('Time (seconds)')
ylabel('pointing error (deg)')

subplot(2,3,5) %plot of velocity error with respect to time
plot(timeArray,velocityArray, timeArray, delOmega*180/pi, '--', timeArray, -
    delOmega*180/pi, '--')
axis([0 simTime -5*delOmega*180/pi 5*delOmega*180/pi])
xlabel('Time (seconds)')
ylabel('velocity (deg/s)')



\end{code}
```

APPENDIX C

MATLAB ATTITUDE CONTROL MODEL USING REACTION WHEELS

```
\begin{code}

%function [] = attitude()
%
%Filename:attitude.m
%Author: Paul D. Friz
%Contact: pdfriz@gmail.com
%Advisor: Joshua L. Rovey (roveyj@mst.edu)
%Affiliation: Missouri University of Science and Technology, Aerospace
%Plasma Lab, Aerospace Enigneering Dept
%Purpose: Models the pointing capabilities of cubeSats using reaction
%wheels
%Detailed Description: attitude.m models the pointing capabilites of a
%cubeSat being controlled by a single axis reaction wheel in the presence
%of Solar Radiation Pressure (SRP) and frictional forces acting on the
%reaction wheel. The assumptions of the model are:
%1.  There are no outside forces affecting the rotation of the space craft
%other than SRP and the reaction wheel
%2.  The spacecraft always knows its current angular position and angular
%velocity with perfect accuracy
%3.  SRP causes a constant torque in only one direction and is calculated
%for the "worst case senario" where the sun is directly hitting one face of
%the cubeSat, that face is half shaded, and the illuminated half of the
%spacecraft is perfectly reflecting sun light back toward the sun.
%4.  The reaction wheel is operated in "minimum torque mode" where only
%enough torque is placed on it to change its RPMs by the minimum amount
%possible.
%5.  Spacecraft is a cube with constant density
%Spacecraft inputs are its size and mass. The reaction wheel inputs are
%its moment of intertia, the minimum amount that the RPMs of the wheel can
%be changed, coulomb coefficient of friction, and viscous coefficient of
%friction (friction proportional to velocity of reaction wheel). By
%changing the initial velocity/angular position as well as the set angular
%position the simulated space craft can be commanded to hold position or
%move to a different attitude.
%

%conversions
RPMtoRadPS = 2*pi/60; %rev per min to rad/s
RadPStoRPM = 60/(2*pi); %rad/s to RPMs
DegtoRad = pi/180; %degrees to radians
RadtoDeg = 180/pi; %radians to degrees

%Spacecraft parameters
M = 2; %Wet mass of cubesat (kg)
s = .1; %length of side of cube sat (m)
```

```
SA = s^2; %surface area of one face of the sat (m^2)

%Reaction Wheel parameters
I = .05*.02^2; %moment of inertia of reaction wheel (Kg*m^2) (50g 20mm
    radius)
delRPM = 1; %minimum amount the reaction wheel can change its angular
    velocity (RPM)
delOmegaRW = delRPM*RPMtoRadPS; %smallest amount the reaction wheel can
    change its angular velocity (rad/s)
omegaRWo = 50; %innitial angular velocity of reacthion wheel (RPMs)
omegaRW = omegaRWo*RPMtoRadPS; %angular velocity of reaction wheel (rad/s)
reactionTime = .1; %how long it takes the reaction wheel to change angular
    velocity by delRPM (s)
Nc = 0; %Coulomb friciton coefficient(N*m)
Fv = 0; %viscous friction coefficient(N*m/RPM)

%Calculated parameters
Icube = (M*s^2)/6; %moment of inertia of cube sat (kg*m^2)
delOmega = I*delOmegaRW/Icube; %the smallest change in angular velocity
    possible for sat.(rad/s)
alphaSat = delOmega/reactionTime; %angular acceleration of the sat due to
    reaction wheels (rad/s^2)
delTheta = .5*alphaSat*reactionTime^2; %angle the sat rotates during
    reaciton time only due to acceleration of RW (rad)

%Attitude parameters/innitial conditions
setAtt = (0)*DegtoRad; %set/desired attitude in rad (parenthetical input in
    deg)
Att0 = 5; %starting attitude (deg)
curAtt = Att0*DegtoRad; %current attitude (rad)
omegaSato = 0; %starting angular velocity of sat in (deg/s)
omegaSat = omegaSato*DegtoRad; %current angular velocity of sat in (rad/s)
switchTheta = (.1)*DegtoRad; %the switching interval in rad (parenthetical
    input in deg)
torqueSat = Icube*alphaSat; %torque on the sat from the reaction wheels (N*m
    )

%worst case senario solar radiation pressure torque. Assuming sun is sining
%directly upon one face of the cube sat, that face is perfectly
%reflective and half of it is shaded.
Fe = 1360; %solar flux constant (W/m^2)
c = 2.99792458e8; %speed of light (m/s)
P = Fe/c; %Solar Radiation Pressure SRP (N/m^2)
Fs = 2*P*SA/2; %solar radiation force assuming all light is reflected 180deg
     (N)
tSolar = Fs*s/4; %torque caused by half of a side of the sat being
```

```
    illuminated (N*m)
alphaSolar = tSolar/Icube; %acceleration due to solar radiation pressure (
    rad/s)
disDelTheta = .5*alphaSolar*reactionTime^2; %angle sat rotates due to SRP
    during raction time (rad)
disDelOmega = alphaSolar*reactionTime; %the change in angular velocity due
    to disturbance torques. (rad/s)

iterations = 1000; %number of iterations of simulation
simTime = iterations*reactionTime; %the time of the simulation (s)
positionArray = zeros(1,iterations); %creating array to store postion data
velocityArray = zeros(1,iterations); %creating array to store velocity data
timeArray = zeros(1,iterations); %creating an array to store time values.
RWRPMArray = zeros(1,iterations); %array to store the current RPMs of the
    reaction wheel
errorArray = zeros(1,iterations); %array to store error values
torqueArray = zeros(1,iterations); %array to store torque values

stop = 0;%innitilize stop value
status = 1;
for t=1:iterations; %t is the simulation timer
    errorTheta = curAtt - setAtt; %the difference between the current
        attitude and the set attitude
    thetaStop = .5*omegaSat^2/alphaSat; %the minimum angular distance it will
         take the satellite to stop rotating at its current angular speed
        assuming constant decelleration
    if abs(errorTheta) > switchTheta + .1*switchTheta %check to see if the
        craft is within 10% of switchTheta
        status = 0; % if position > 10% out of switchTheta then thrusters are
             not keeping craft stable enough
    end

    if sign(errorTheta) == sign(omegaSat)
        stop = 0;
    end
    if abs(errorTheta) <= switchTheta
        stop = 0;
        if abs(omegaSat) >= delOmega && omegaSat > 0 && errorTheta > 0 %kill
            + velocity inside of switchInt
            torque = - torqueSat;
        elseif abs(omegaSat) >= delOmega && omegaSat < 0 && errorTheta < 0 %
            kill - velocity inside of switchInt
            torque = + torqueSat;
        else
            torque = 0;
        end
```

```
elseif errorTheta > switchTheta %when "above" the switchInt
    if errorTheta < thetaStop && omegaSat < 0 && stop == 0 %give signal
        to stop if moving fast enough to overshoot
        stop = 1;
        torque = + torqueSat;
    elseif stop == 1 && errorTheta < thetaStop %stoping
        torque = + torqueSat;
    elseif stop == 1 && errorTheta >= thetaStop %costing toward desired
        attitude to avoid stopping short
        torque = 0;
    else %accelerate toward desired theta
        torque = - torqueSat;
    end
elseif errorTheta < -1*switchTheta %when "below" the switching interval
    if errorTheta > -1*thetaStop && omegaSat > 0 && stop == 0 %give
        command to stop to prevent overshooting
        stop = 1;
        torque = - torqueSat;
    elseif stop == 1 && errorTheta > -1*thetaStop %stopping
        torque = - torqueSat;
    elseif stop == 1 && errorTheta <= -1*thetaStop %costing to avoid
        stopping short
        torque = 0;
    else %accelerate toward desired theata
        torque = + torqueSat;
    end
else
    torque = 0;
end

%effects of reaction wheel friction
Nf = Nc*sign(omegaRW) + Fv*omegaRW*RadPStoRPM; %torque due to friction
af = -Nf/I; %acceleration of reaction wheel due to friciton
delOmegaRWf = af*reactionTime; %change in ang vel of RW due to friction
delOmegaf = I*delOmegaRWf/Icube; %change in ang vel of sat due to RW
    friction
alphaSatf = delOmegaf/reactionTime; %ang acc of the sat due to reaction
    wheel friction
delThetaf = .5*alphaSatf*reactionTime^2; %ang dist the sat moves from the
     acceleration of the reaction wheel friction

if torque == torqueSat %reaction wheel moving to create positive torque
    on spacecraft
    curAtt = curAtt + delTheta + disDelTheta + delThetaf + omegaSat*
        reactionTime;
    omegaSat = omegaSat + delOmega + disDelOmega - delOmegaf;
```

```
        omegaRW = omegaRW - delOmegaRW + delOmegaRWf;
    elseif torque == -torqueSat %reaction wheel moving to create negative
        torque on spacecraft
        curAtt = curAtt - delTheta + disDelTheta + delThetaf + omegaSat*
            reactionTime;
        omegaSat = omegaSat - delOmega + disDelOmega - delOmegaf;
        omegaRW = omegaRW + delOmegaRW + delOmegaRWf;
    else %reaction wheel remaining stationary (other than friction)
        curAtt = curAtt + disDelTheta + delThetaf + omegaSat*reactionTime;
        omegaSat = omegaSat + disDelOmega - delOmegaf;
        omegaRW = omegaRW + delOmegaRWf;
    end

    positionArray(1,t) = curAtt*RadtoDeg; %converted back to deg
    velocityArray(1,t) = omegaSat*RadtoDeg; %converted back to deg/s
    timeArray(1,t) = t*reactionTime;
    RWRPMArray(1,t) = omegaRW*RadPStoRPM;
    errorArray(1,t) = errorTheta*RadtoDeg;
    torqueArray(1,t) = torque;
end

display(status)

figure
subplot(2,3,1); %spacecraft attitude plot
plot(timeArray,positionArray)
xlabel('Time (seconds)')
ylabel('angular position(deg)')

subplot(2,3,2); %spacecraft velocity plot
plot(timeArray,velocityArray)
xlabel('Time (seconds)')
ylabel('angular velocity (deg/s)')

subplot(2,3,3) %torque plot
plot(timeArray, torqueArray)
xlabel('Time (seconde)')
ylabel('torque N*m')

subplot(2,3,4) %error plot
plot(timeArray,errorArray, timeArray, switchTheta*180/pi, '--', timeArray, -
    switchTheta*180/pi, '--')
axis([0 simTime -5*switchTheta*180/pi 5*switchTheta*180/pi])
xlabel('Time (seconds)')
ylabel('pointing error (deg)')
```

```
subplot(2,3,5) %plot of velocity error with respect to time
plot(timeArray,velocityArray, timeArray, delOmega*180/pi, '--', timeArray, -
    delOmega*180/pi, '--')
axis([0 simTime -5*delOmega*180/pi 5*delOmega*180/pi])
xlabel('Time (seconds)')
ylabel('velocity (deg/s)')

subplot(2,3,6); %reaction wheel RPM plot
plot(timeArray,RWRPMArray)
xlabel('Time (seconds)')
ylabel('RPM of reaction wheel')


\end{code}
```

REFERENCES

[1] E. Moreau. Airflow control by non-thermal plasma actuators. *Journal of Physics D: Applied Physics*, 40:605–636, 2007.

[2] K. Ramakumar and J. Jacob. Flow control and lift enhancement using plasma actuators. In *AIAA Fluid Dynamics Conference and Exhibit*, Toronto, Ontario Canada, 2005. AIAA, Paper 2005–4635.

[3] A. Santhanakrishnan, Nan Jou Pern, K. Ramakumar, Andrew Simpson, and J. D. Jacob. Enabling flow control technology for low speed uavs. In *AIAA Infotech@Aerospace*, Arlington, Virginia, September 2005. AIAA, Paper 2005–6960.

[4] Thomas C. Corke, C. Lon Enloe, and Stephen P.Wilkinson. Dielectric barrier discharge plasma actuators for flow control. *Annual Review of Fluid Mechanics*, 42: 505–529, 2010.

[5] Jignesh Soni and Subrata Roy. Low pressure characterization of dielectric barrier discharge actuators. *Applied Physics Letters*, 102(112908):1–5, 2013.

[6] Takashi Abe, Yuji Takizawa, Shunichi Sato, and Nobara Kimura. Experimental study for momentum transfer in a dielectric barrier discharge plasma actuator. *AIAA*, 46(9): 2248–2256, 2008.

[7] Timothy G. Nichols and Joshua L. Rovey. Surface potential and electric field measurements in plasma actuators at low pressure. *AIAA*, 51(5):1054–1065, 2013.

[8] Timothy G. Nichols and Joshua L. Rovey. Fundamental processes of dbd plasma actuators operating at high altitude. In *50th Aerospace Sciences Meeting*, Nashville, TN, 2012. AIAA-2012-0822.

[9] C. L. Enloe, T. E. McLaughlin, Robert D. VanDyken, K. D. Kachner, Eric J. Jumper, and Thomas C. Corke. Mechanisms and responses of a single dielectric barrier plasma actuator: Plasma morphology. *AIAA*, 42(3):589–594, 2004.

[10] C. L. Enloe, T. E. McLaughlin, Robert D. VanDyken, K. D. Kachner, Eric J. Jumper, Thomas C. Corke, M. Post, and O. Haddad. Mechanisms and responses of a single dielectric barrier plasma actuator: Geometric effects. *AIAA*, 42(3):595–604, 2004.

[11] M. L. Juan, M. Righini, and R. Quidant. Plasmon nano-optical tweezers. *Nature Photonics*, 5(6):349–356, 2011.

[12] J. A. Schuller, E. S. Barnard, W. Cai, Y. C. Jun, J. S. White, and M. L. Brongersma. Plasmon nano-optical tweezers. *Nature Photonics*, 5(6):349–356, 2011.

[13] X. Yang, Y. Liu, R. F. Oulton, X. Yin, and X. Zhang. Optical forces in hybrid plasmonic waveguides. *Nano Letters*, 11(2):321–328, 2011.

[14] K. Wang, E. Schonbrun, and K. B. Crozier. Propulsion of gold nanoparticles with surface plasmon polaritons: Evidence of enhanced optical force from near-field coupling between gold particle and gold film. *Nano Letters*, 9(7):2623–2629, 2009.

[15] Meredith Gibb. Lisa laser interferometer space antenna project office. `http://lisa.nasa.gov/`. Accessed: 2014-04-17.

[16] Lisa: Study of the laser interferometer space antenna, final technical report. *astrium*, 13631/99/NL/MS(LI-RP-DS-009), 2000.

[17] NASA and esa. Laser interferometer space antenna (lisa) mission concept. (LISA-PRJ-RP-0001), 2009.

[18] Kenneth Carpenter. Si: The stellar imager. `http://hires.gsfc.nasa.gov/si/`. Accessed: 2014-04-17.

[19] Jorgen Christensen-Dalsgaard, Kenneth G Carpenter, Carlus J Schrijver, Margarita Karovska, and the SI Team. The stellar imager (si) - a mission to resolve stellar surfaces, interiors, and magnetic activity. *Journal of Physics: Confrence Series*, 271 (012085), 2011.

[20] Kenneth G. Carpenter *et. al*. Si-the stellar imager: A uv/optical deep-space telescope to image stars and oberve the universe with 0.1 milli-arcsec angular resolution. 2005.

[21] C. L. Enloe, G.I. Font, T. E. McLaughlin, and D. M. Orlov. Surface potential and longitudinal electric field measurements in the aerodynamic plasma actuator. *AIAA*, 46(11):2730–2739, 2008.

[22] C. L. Enloe, M. G. McHarg, and T. E. McLaughlin. Time-correlated force production measurements of the dielectric barrier discharge plasma aerodynamic actuator. *Journal of Physics D: Applied Physics*, 103, 2008.

[23] James W. Gregory, C. Lon Enloe, Gabriel I. Font, and Thomas E. McLaughlin. Force production mechanisms of a dielectric-barrier discharge plasma actuator. In *45th AIAA Aerospace Sciences Meeting and Exhibit*, Reno, Nevada, 2007. AIAA, Paper 2007-185.

[24] John W. Dunning and John M. Sankovic. NasaâĂŹs electric propulsion program. In *35th AIAA/ASME/SAE/ASEE Joint Propulsion Conference and Exhibit*, Los Angeles, California, 1999. AIAA-99-2161.

[25] Armen Toorian, Ken Diaz, and Simon Lee. The cubesat approach to space access. (1135), 2008.

[26] Peter Fortescue, John Stark, and Graham Swinerd. *Spacecraft Systems Engineering*. Wiley, 2003.

[27] James R. Wertz. *Spacecraft Attitude Determination and Control*. Graphics Press, 1985.

[28] Eugene Hecht. *Optics*. Addison-Wesley, fourth edition, 2002.

[29] David J. Griffiths. *Introduction to Electrodynamics*. Prentice Hall, third edition, 1999.

[30] David A. Vallado. *Fundamentals of Astrodynamics and Applications*. Microcosm Press, fourth edition, 2013.

[31] James R. Wertz and Wiley J. Larson, editors. *Space Mission Analysis and Design*. Space Technology Library, third edition, 1999.

[32] E. Gill, P. Sundaramoorthy, J. Bouwmeester, B. Zandbergen, and R.Reinhard. Formation flying within a constellation of nano-satellites: The qb50 mission. *Acta Astronautica*, 82(1):110–117, 2013.

[33] Juergen Mueller, Richard Hofer, and John Ziemer. Survey of propulsion technologies applicable to cubesats. *Jet Propulsion Laboratory*, 2010.

[34] Thomas A. Moore. *Six Ideas That Shaped Physics, Unit N: The Laws of Physics are Universal*. McGraw-Hill, second edition, 2003.

[35] Thomas A. Moore. *Six Ideas That Shaped Physics, Unit C: Conservation Laws Constrain Interactions*. McGraw-Hill, second edition, 2003.

[36] George P Sutton and Oscar Biblarz. *Rocket Propulsion Elements*. John Wiley & Sons, Inc., eighth edition, 2010.

[37] Th. Kwaaitaal. Contribution to the interferometric measurement of sub-angstrom vibrations. *AIP Review of Scientific Instruments*, 45(1):39–41, 1974.

[38] R.G. Klaver, L.M. Krieg, and J.J.M. Braat. Measuring absolute optical path differences with angstrom accuracy over ranges of millimeters. In *Proceedings Symposium IEEE/LEOS Benelux Chapter*, Delft, The Netherlands, 2000. Delft University of Technology.

[39] Thomas A. Moore. *Six Ideas That Shaped Physics, Unit Q: Particles Behave Like Waves*. McGraw-Hill, second edition, 2003.

[40] Wilam E. Wiesel. *Spaceflight Dynamics*. Aphelion Press, third edition, 2010.

[41] Marcel J. Sidi. *Spacecraft Dynamics and Control: A Practical Engineering Approach*. Cambridge University Press, third edition, 1997.

[42] Richard C. Dorf and Robert H. Bishop. *Modern Control Systems*. Prentice Hall, ninth edition, 2000.

[43] Boris Lamontagne and Py Christophe. Microblinds and a method of fabrication thereof, 09 2006. URL `http://www.freepatentsonline.com/y2006/0196613.html`.

[44] Taisen Zhuang, Alexey Shashurin, Isak Beilis, and Michael Keidar. Ion velocities in a micro-cathode arc thruster. *Physics of Plasmas*, 19(063501), 2012.

[45] Alexey Shashurin, Michael Keidar, and Taisen Zhuang. Comparative analysis of micro-cathode arc thruster performance. In *33rd International electric Propulsion Conference*, Washington D.C., 2013. IEPC, Paper 2013-389.

[46] Michael Keidar, Samudra Haque, Taisen Zhuang, Alexey Shashurin, Dereck Chiu, and George Teel. Micro-cathode arc thruster for phonesat propulsion. In *27th Annual AIAA/USU Conference on Small Satellites*, Logan, Utah, 2013. Paper SSC13-VII-9.

[47] Taisen Zhuang, Alexey Shashurin, Samudra Haque, and Michael Keidar. Performance characterization of the micro-cathode arc thruster and propulsion system for space applications. In *46th AIAA Joint Propulsion Conference and Exhibit*, Nashville, TN, 2010. AIAA 2010-7018.

[48] Alameda Applied Sciences Corporation. `http://www.aasc.net/micropropulsion/vat/vat-specifications`. Accessed: 2014-04-17.

[49] J. Schein, N. Qi, R. Binder, M. Krishnan, J. K. Ziemer, J. E. Polk, and A. Anders. Inductive energy storage driven vacuum arc thruster. *Review of Scientific Instruments*, 73(2):925–927, 2002.

[50] Tamer Akan, Serdar Demirkol, Naci Ekem, Suat Pat, and Geavit Musa. Study of metal and ceramic thermionic vacuum arc discharges. *Plasma Science and Technology*, 9 (3):280–283.

[51] Jochen Schein, Niansheng Qi, Robert Binder, Mahadevan Krishahnan, John Ziemer, James Polk, and Andre Anders. Low mass vacuum arc thruster system for station keeping missions. In *IEPC-01-228*, Pasadena, CA, 2001. International Electric Propulsion Confrence.

[52] M. Coletti, F. Guarducci, and S. B. Gabriel. A micro ppt for cubesat application: Design and preliminary experimental results. *Elsevier*, 69:200–208, 2011.

[53] Clyde Space and Mars Space LTD. `http://www.clyde-space.com/cubesat_shop/propulsion/303_cubesat-pulse-plasma-thruster`. Accessed: 2013-11-18.

[54] L. F. Velasquez-Garcia, A. I. Akinwande, and M. Martinez-Sanchez. A planar array of micro-fabricated electrospray emitters for thruster applications. *Journal of Microelectromechanical Systems*, 15(5):1272–1280, 2006.

[55] F. Martel and P. Lozano. Ion electrospray thruster assemblies for cubesats. In *iCubeSat Workshop*, Cambridge, 2012. Massachusetts Institute of Technology.

[56] J. Mueller, J. Ziemer, R. Hofer, R. Wirz, and T. O. Donnell. A survey of micro-thrust propulsion options for microspacecraft and formation flying missions. In *CubeSat 5th Annual Developers Workshop*, San Luis Obispo, CA, 2008. California Polytechnic State University.

[57] Tom Roy, Vlad Hruby, Nathan Rosenblad, Peter Rostler, and Douglas Spence. Cubesat propulsion using electrospray thrusters. In *23rd Annual AIAA/USU Conference on Small Satellites*. SSC09-II-6, 2009.

[58] Blue Canyon Technologies. `www.bluecanyontech.com`. Accessed: 2014-04-17.

[59] Wei Wu, Dibyendu Dey, Omer G. Memis, Alex Katsnelson, and Hooman Mohseni. Fabrication of large area periodic nanostructures using nanosphere photolighography. *Nanoscale Res Lett*, 3:351–354, 2008.

[60] C.L. Cheung, R.J. Nikolic, C.E. Reinhardt, and T.F. Wang. Fabrication of nanopillars by nanosphere lithography. *Nanotechnology*, 17(5):1339–1343, 2006.

[61] John C. Hulteen and Richard P. Van Duyne. Nanosphere lithography: A materials general fabrication process for periodic particle array surfaces. *American Vacuum Society*, 13(3):1553–1558, 1995.

VITA

Paul Friz was raised in St. Louis, Missouri, and was home schooled until high school where he attended Westminster Christian Academy graduating in 2008. From a young age he has been fascinated by science, particularly astronomy, physics, and space exploration. At the age of 14 he saved up a summers worth of lawn mowing money to buy a telescope. Planning on eventually becoming an astrophysicist he attended Truman State University in Kirksville, Missouri, graduating in December 2012 with a Bachelor of Science in Physics and minors in Mathematics and Music. However, being frustrated that, despite great technical advancements, humans have not explored beyond low earth orbit since 1972 he decided to become an aerospace engineer instead. As of May 2014 he has graduated from the Missouri University of Science and Technology with a Master of Science degree in aerospace engineering. He hopes to work as an engineer for NASA or a private space company in order to promote manned exploration and colonization of the solar system and beyond.

In his spare time Paul enjoys photography, particularly astrophotography, playing violin, hiking, biking, skydiving, playing Kerbal Space Program and Settlers of Catan, listening to audio books, drinking craft root beers, learning new things, and exploring. He would like to move to the moon or mars someday if that becomes a possibility, but in the meantime the earth is a pretty cool planet and there is plenty of it which he has not explored yet.